General Disclaimer

One or more of the Following Statements may affect this Document

- This document has been reproduced from the best copy furnished by the organizational source. It is being released in the interest of making available as much information as possible.

- This document may contain data, which exceeds the sheet parameters. It was furnished in this condition by the organizational source and is the best copy available.

- This document may contain tone-on-tone or color graphs, charts and/or pictures, which have been reproduced in black and white.

- This document is paginated as submitted by the original source.

- Portions of this document are not fully legible due to the historical nature of some of the material. However, it is the best reproduction available from the original submission.

A STUDY OF THE EFFECT OF THE ELECTROMAGNETIC INTERACTION BETWEEN THE MOON AND THE SOLAR WIND

By Dr. K. Schwartz

December, 1969

Prepared Under Contract No. NAS 2-5153

By

AMERICAN NUCLEONICS CORPORATION
1007 AIR WAY
GLENDALE, CALIFORNIA 91201

For

AMES RESEARCH CENTER
NATIONAL AERONAUTICS AND
SPACE ADMINISTRATION

NASA CR _____

A STUDY OF THE EFFECT OF THE ELECTROMAGNETIC INTERACTION BETWEEN THE MOON AND THE SOLAR WIND

By Dr. K. Schwartz

December, 1969

Prepared Under Contract No. NAS2-5153 by

American Nucleonics Corporation
1007 Air Way
Glendale, California 91201

for

AMES RESEARCH CENTER
NATIONAL AERONAUTICS AND SPACE ADMINISTRATION

TABLE OF CONTENTS

TABLE OF CONTENTS

LIST OF ILLUSTRATIONS

LIST OF ILLUSTRATIONS

1.0 Introduction

Under Contract NAS2-5153 with NASA-Ames Research Center, American Nucleonics Corporation has participated with NASA scientists in the investigation of the electromagnetic interaction of the solar wind with the moon. These investigations cover both the DC and time dependent interactions. They were initiated to provide a theoretical framework through which the experimental data obtained from the Explorer 35 magnetometer and the Apollo 12 ALSEP magnetometer can be interpreted and correlated. The DC interaction has also been proposed as a possible mechanism for providing an intense heating phase during the initial development of the solar system (Sonett, Colburn and Schwartz, 1968, and Sonett, Colburn, Schwartz and Keil, 1969). This mechanism could provide an alternative to extinct radioactive heating as a source of as yet unexplained melting and cooling details of meteorites.

Preliminary details of the unipolar induction heating were published in 1968 (Sonett, Colburn and Schwartz, 1968). A more detailed work is currently in press (Sonett, Colburn, Schwartz and Keil, 1969). The main driving source for the unipolar induction generator

in both cases is a simplistic model of a T Tauri proto sun. In Section 2.0, this model is compared with more general details of T Tauri stars and the related spin down and driving magnetic fields. An alternative model for the T Tauri environment is proposed. This alternative model tends to have higher driving fields, and higher momentum and energy flux during the period when intense planetary heating can occur. Because of these possibilities, further investigation is carried out into the possibility of relaxing the high hohlraum temperature condition and still obtaining high heating rates. It is found that for hohlraum temperatures as low as 200 degrees centigrade an intense heating phase can exist. With a moderate increase (a factor of 10) in the driving field, an intense heating phase is found to exist for hohlraum temperatures down to at least 100°C. These results were obtained for an olivine electrical conductivity (Rikitake, 1966). For a material with somewhat higher conductivity at low temperatures, a period of intense heating might occur for hohlraum temperatures down to 0°C even without the higher driving fields assumed in the alternative model of the T Tauri environment.

Section 3.0 describes the theoretical investiga-

tion into the response of a two layer moon to an incident CW electromagnetic field. The investigation begins with the coupled magnetic and V x B electric field in the frame of reference in the moon. The original results of Blank and Sill (1969) are recovered at the low frequency limit, but it is shown that their solution is but one half of the total solution to the problem. In the DC limit, the unipolar induction generator solutions are obtained.

In Section 4.0 of this report, the two layer unipolar induction generator is used as a model for investigating, parametrically, the ranges of surface and interior lunar conductivities which are compatible with the magnetometer data from Explorer 35 (Colburn et al, 1967 and Ness et al, 1967). Using the definition of the k factor (Sonett and Colburn, 1967 and 1968) and the lack of an observed lunar bow shock, limits are placed on the possible combinations of internal and surface electrical conductivities. It is also shown that within these limits there is sufficient leeway to provide for an incipient standoff of the solar wind near the lunar limb.

In Section 5.0 a simple investigation is outlined into the use of the thermal history computer program

in determining the cooling rate of a free radiating surface. A simple criterion is given relating the time scale of interest to the array spacing for the distance integration.

2.0 Early Planetary Heating by a T Tauri Driven Unipolar Generator

Sonett et al (1968) have suggested that a unipolar induction generator driven by a T Tauri solar wind could account for the early heating which is required to explain the apparent melting and differentiation of meteoritic bodies. In this section, the T Tauri phase conditions will be examined as they apply to the solar spin rate, solar magnetic field and the mass flux rate. Starting from the angular momentum conservation equation for a spherical system first derived by Mestel (1967), we will present the early time conditions which have been used for the T Tauri heating calculations to this time. Next, following Schwartz and Schubert (1969), we will examine some general effects which can be determined from angular momentum conservation when the theoretical results of Iben (1965) and Roxburgh (1966) are combined with the observational data of Kuhi (1964). Finally, still using the angular momentum conservation equation, we will examine a possible alternative to the original, hypothetical T Tauri environment. In conjunction with the alternative, we will consider the effect on planetary heating when the driving electric field (VXB) is increased and the hohlraum

temperature at planetary formation is decreased.

2.1 The Original Hypothetical T Tauri Environment

The original zero time environment for the sun was obtained on the basis of a 4.5 eon (1 eon = 10^9 years) solar age. The solar wind number density, n_{sw}, and solar wind velocity, v_{sw}, were assumed to be given by the equations:

$$n_{sw} = n_p e^{-\lambda_{ns}(t-4.5)} \tag{1}$$

$$v_{sw} = v_p e^{-\lambda_{vs}(t-4.5)} \tag{2}$$

where the time is in units of eons, n_p and v_p are the present day number density and velocity of the solar wind and λ_{ns} and λ_{vs} are the respective time constants. The present day values of n_p and v_p were taken as:

$$n_p = 10^7 \text{ protons/m}^3 \tag{3}$$

$$v_p = 4 \times 10^5 \text{ meters/sec} \qquad (4)$$

and λ_{ns} and λ_{vs} were assumed to be:

$$\lambda_{ns} = 1.0214 \text{ eons}^{-1} \qquad (5)$$

$$\lambda_{vs} = 0.2441 \text{ eons}^{-1} \qquad (6)$$

The values for n_p and v_p are at 1 a.u., i.e. at the earth's orbit. The zero time values of number density and velocity are thus:

$$n_{sw}(o) = 10^9 \text{ protons/m}^3 \qquad (7)$$

$$v_{sw}(o) = 1.2 \times 10^6 \text{ meters/sec} \qquad (8)$$

The enhanced solar wind was then incorporated into a solar despin theory which, in a simple form, can be derived from the angular momentum conservation equation

due to Mestel (1968). For a star of mass M, radius R and moment of inertia kMR^2, the angular momentum equation is:

$$\frac{d}{dt}\left(kM\Omega R^2\right) = \frac{2}{3}\,\Omega_A r_A^2\,\frac{dM}{dt} \qquad (9)$$

where Ω is the angular velocity of the star, r_A is the radius of some surface ($r_A \geq R$) beyond which the mass ejected from the star no longer interacts with the star and Ω_A is the angular velocity of the ejected mass at r_A. In this report it will be assumed that the ejected mass and the star corotate, $\Omega = \Omega_A$ for $r \leq r_A$ In the theory as derived by Modisette, the moment of inertia (kMR^2) is assumed constant through the entire period of interest. The mechanism which produces the corotation is the magnetic field and the corotation ceases when the mass flow becomes super Alfvénic. Once the solar wind is beyond the coronal expansion, the velocity v_{sw} is constant, v_A. The Alfvénic speed v_A is related to the local magnetic field B by the relation

$$v_A^2 = \frac{B_A^2}{\rho_A \mu_o} \qquad (10)$$

where ρ_A is the mass density at r_A and $\mu_o = 4\pi \times 10^{-7}$.

It is further assumed that

$$B_A = B_s \, (R/r_A)^2 \qquad (11)$$

where B_s is the magnetic field at the solar surface, R. With these assumptions, Equation (9) can be integrated to give:

$$\Omega(t) = \Omega_p \exp \left\{ - \frac{8\pi}{3I} R^4 \int_{4.5}^{t} (B_s^2/v_A) dt \right\} \qquad (12)$$

where Ω_p is the present day solar spin rate, $\Omega_p = 2.87 \times 10^{-6}$ radians/sec, and I is the present day value for the solar moment of inertia, $I \sim 6 \times 10^{46}$ kilogram-meters^2. If now it is further assumed that

$$B_s = B_{sp}\, e^{-\gamma(t-4.5)} \quad , \; B_{sp} \sim 3 \text{ gauss} \tag{13}$$

and this and Equation (2) are inserted into (12), the time dependence for the solar spin rate becomes

$$\Omega(t) = \Omega_p e^{A(t)} \tag{14}$$

$$A(t) = \frac{.1827}{2\gamma - \lambda_{vs}} \left\{ \exp\left((4.5-t)(2\gamma-\lambda_{vs})\right) - 1 \right\} \tag{15}$$

under the assumption that the solar mass and the solar radius remain constant during the despinning with their present day values. The break up or critical angular velocity of the sun is 4.2×10^{-4} radians per second. This value puts an upper limit on the value of γ :

$$0 \leq \gamma \leq .448/\text{eon} \tag{16}$$

After the initial proto-planetary heating computer program had been completed, it was noted that the enhanced solar wind, as described by Equations (1) and (2), had neither sufficient momentum flux to prevent a lunar bow shock and, hence, k factor limiting (see Sonett and Colburn (1967 & 1968) for a description of k factor limiting) nor sufficient energy flux to produce significant heating.

In order to increase both the momentum flux and energy flux, the decision was then made to include a T Tauri mass flow in the initial solar wind. Extrapolating from the data presented by Kuhi (1964), a very simple T Tauri mass flow was superimposed on the original solar wind model. It was assumed that the mass of the sun followed a time history of the form:

$$M_s = M_\odot(1 + .5\ e^{-\alpha t}) \qquad (17)$$

$$\alpha = \lambda_{vT} + \lambda_{nT} = 1285.5/\text{eon} \qquad (18)$$

where λ_{vT} and λ_{nT} are the time constants coupled with the T Tauri flow velocity and density at one a.u.:

$$v_T = v_{To}\, e^{-\lambda_{vT} t} \tag{19}$$

$$n_T = n_{To}\, e^{-\lambda_{nT} t} \tag{20}$$

with

$$n_{To} = 4.3 \times 10^{14} \text{ protons/m}^3 \tag{21}$$

$$v_{To} = 2 \times 10^5 \text{ m/s} \tag{22}$$

$$\lambda_{vT} = 85.5/\text{eon} \tag{23}$$

$$\lambda_{nT} = 1200/\text{eon} \tag{24}$$

The method for obtaining the spin rate, using the magnetically controlled spin down theory of Modisette, however, was not altered. It will be shown later that the resultant driving electric field can be considered as a lower limit to the driving fields derived from other models. Further, the velocity profile for the added T Tauri flow assumes a cooler corona rather than that assumed at the beginning of this section.

2.2 Early Solar Despinning

In the preceding section, the original early time solar environment model was described. This model has been used to obtain data for the proto-planetary heating process discussed by Sonett, Colburn and Schwartz (1968) and Sonett, Colburn, Schwartz and Keil (1969). Because of certain logical inconsistencies in the early time solar environment model, an investigation was begun into possible alternatives, especially to the despinning of the sun.

The present rotation rate of the sun's surface, 2.9×10^{-6} rad/sec, is much smaller than its break up angular velocity, 4.2×10^{-4} rad/sec. Assuming that the sun is in uniform rotation and that it started at its break up angular velocity, it must have lost considerable angular momentum during the course of its evolution. If

the sun is assumed to have passed through a T Tauri-like phase during its contraction, it could have lost considerable angular momentum before nuclear burning commenced. For T Tauri mass loss rates of $0(10^{-8}\ M_\odot/yr)$ (Kuhi 1964), where $M_\odot = 2 \times 10^{33}$ gm , the sun could have despun to rotation rates of $0(10^{-5}$ rad/sec) within tens of millions of years, even without the braking effect of an enhanced solar magnetic field. Kraft (1967) has reported a rate of $0(10^{-5}$ rad/sec) for stars of about 1 solar mass and age 3×10^7 years. Thus, the angular velocity of the sun could have been reduced an order of magnitude below its break up rate at $0(10^7$ yr) (Iben 1965). Subsequent braking by the solar wind could easily reduce the solar angular velocity of the sun to its present value.

To obtain some idea of the despinning effect, it will be assumed that the sun passed through a T Tauri phase during its slow contraction to a stable stage of hydrogen burning. T Tauri stars are characterized by an average mass loss rate of $0(10^{-8}\ M_\odot/yr)$ and photospheric material ejection velocities of $0(10^2$ km/sec) (Kuhi, 1964). It is reasonable to assume that at such an active period

in a star's evolution as the T Tauri stage, there is a corona in which the ejected material is heated and subsequently accelerated in the manner of a solar wind. Since photospheric ejection velocities are $0(10^2$ km/sec), it must be true that at the coronal base of a T Tauri star the velocities are also $0(10^2$ km/sec).

An enhanced solar magnetic field could have existed in the T Tauri stage. Babcock (1958) has placed an upper limit of 10^3 gauss on the magnetic field of T Tauri stars. Even without the additional braking effect of such an enhanced field, the T Tauri mass loss is quite effective in despinning the sun. A spherically symmetric, non-magnetically controlled expansion of the T Tauri wind from its coronal base will be considered.

An estimate of the maximum magnetic field, B, consistent with the assumption of a spherically symmetric expansion can be made by equating the Alfvén speed with the material ejection velocity at the coronal base, $v_s = B_s/(4\pi\rho_s)^{1/2}$ where ρ is the density and the subscript s refers to conditions at the coronal base. Combining this with the mass loss rate $4\pi r_s^2 \rho_s v_s$ (r_s is the radius of the coronal base), one finds:

$$B_s = \left[\frac{131 (\dot{M}/10^{-7}\ M_\odot) v_s}{(r_s/R_\odot)^2} \right]^{1/2} \text{ gauss,} \qquad (25)$$

where in this equation the units of v_s are km/sec, the units of the mass loss rate $\dot{M}$ are gm/yr and $R_\odot = 6.96 \times 10^{10}$ cm . This result is presented in Figure 1, where B_s is shown as a function of v_s with $(M/10^{-7}\ M_\odot)/(r_s/R_\odot)^2$ as a parameter. For a given value of v_s and the parameter, the value of B_s is the maximum magnetic field that could exist at the coronal base if the expansion is not to be magnetically controlled. For T Tauri values of v_s , $\dot{M}$ and r_s , the magnetic field could be as large as 1-100 gauss and the expansion would still be spherically symmetric.

For a star of mass M , radius R and moment of inertia kMR^2 , the angular momentum equation is:

$$\frac{d}{dt} (kM\Omega R^2) = \frac{2}{3} \Omega_s r_s^2 \frac{dM}{dt} \text{ (Mestel 1968)} , \qquad (26)$$

where Ω is the angular velocity. This equation inte-

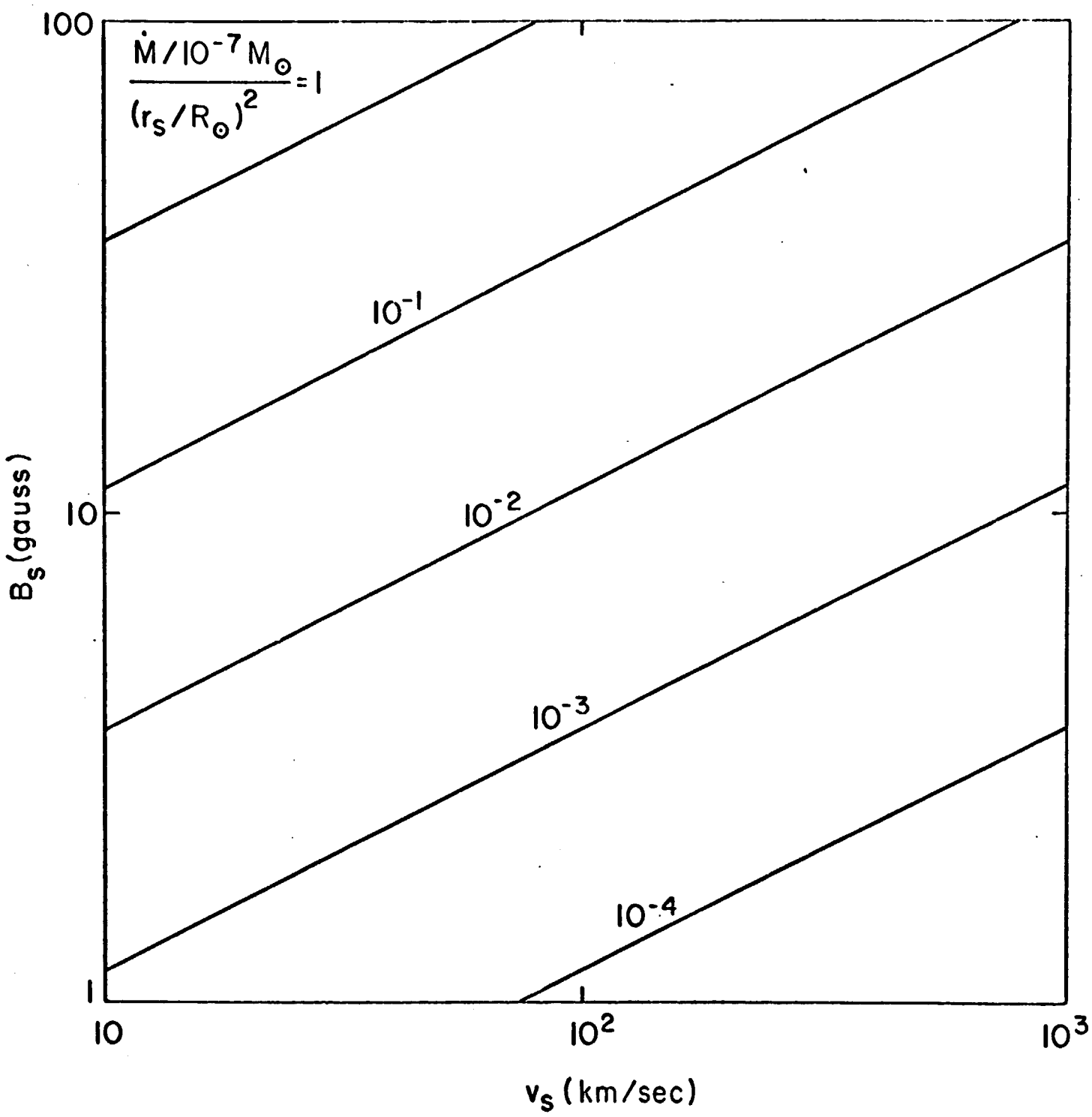

Figure 1

The Maximum Magnetic Field at the Coronal Base B_s vs. the Material Ejection Velocity at the Coronal base v_s for Various Values of $(\dot{M}/10^{-7}M_\odot)/(R_s/R_\odot)^2\ yr^{-1}$.

grates to:

$$\frac{\Omega}{\Omega_i} = \left(\frac{R_i}{R}\right)^2 \left(\frac{M}{M_i}\right)^{\frac{2\alpha^2}{3k} - 1} \qquad (27)$$

where $r_s = \alpha R$, α and k have been assumed constant, Ω_s has been assumed equal to Ω , and the subscript i refers to an initial reference condition in the T Tauri stage. It is assumed that $\Omega_i = (.45\ GM_i/R_i^3)^{1/2}$, the break up angular velocity for the state M_i and R_i , and that at 10^7 years, $M = M_\odot$ and $R = R_\odot$. (Note that G is the gravitational constant). Equation (27) becomes:

$$\Omega(10^7\ \text{yr}) \approx 4 \times 10^{-4} \left(\frac{R_i}{R_\odot}\right)^{1/2} \left(\frac{M_\odot}{M_i}\right)^{\frac{2\alpha^2}{3k} - \frac{3}{2}} \text{sec}^{-1} \qquad (28)$$

It is reasonable to suppose that during the T Tauri stage the sun contracted by a factor of 50. The

ratio of initial to final mass is between 1 and 1.5 for average mass loss rates of $0(10^{-8}\ M_\odot/yr)$ for periods of 10^7 years. The parameter $2\alpha^2/3k - 3/2$ could vary from about 3 to 40 since $\alpha = r_s/R$ is between 1 and 2, and k is .134 for a fully convective star built on the 3/2 polytropic model (Roxburgh 1966) and $k = .06$ for the present sun.

Figure 2 shows a plot of $\Omega(10^7\ yr)$ vs. $2\alpha^2/3k - 3/2$ for several values of $M_i/M_\odot$ and for $R_i/R_\odot = 50$. For mass loss rates in agreement with the observations of Kuhi, the sun is easily spun down to angular velocities of order 10^{-5} rad/sec in 10^7 years. Kraft (1967) has reported such a rotation rate for a solar mass star with an age of several tens of millions of years. A mass loss of 10% is sufficient to despin the sun to critical rotation rates of $0(10^{-4}$ rad/sec) (Mestel 1968) and only a slightly higher mass loss, say about 15%, is needed to despin an additional order of magnitude. Of course, if negligible mass loss is assumed, further despinning could be accomplished by a moderately enhanced magnetic field. Once a stable solar configuration has been reached further despinning can occur according to the model presented in the previous section.

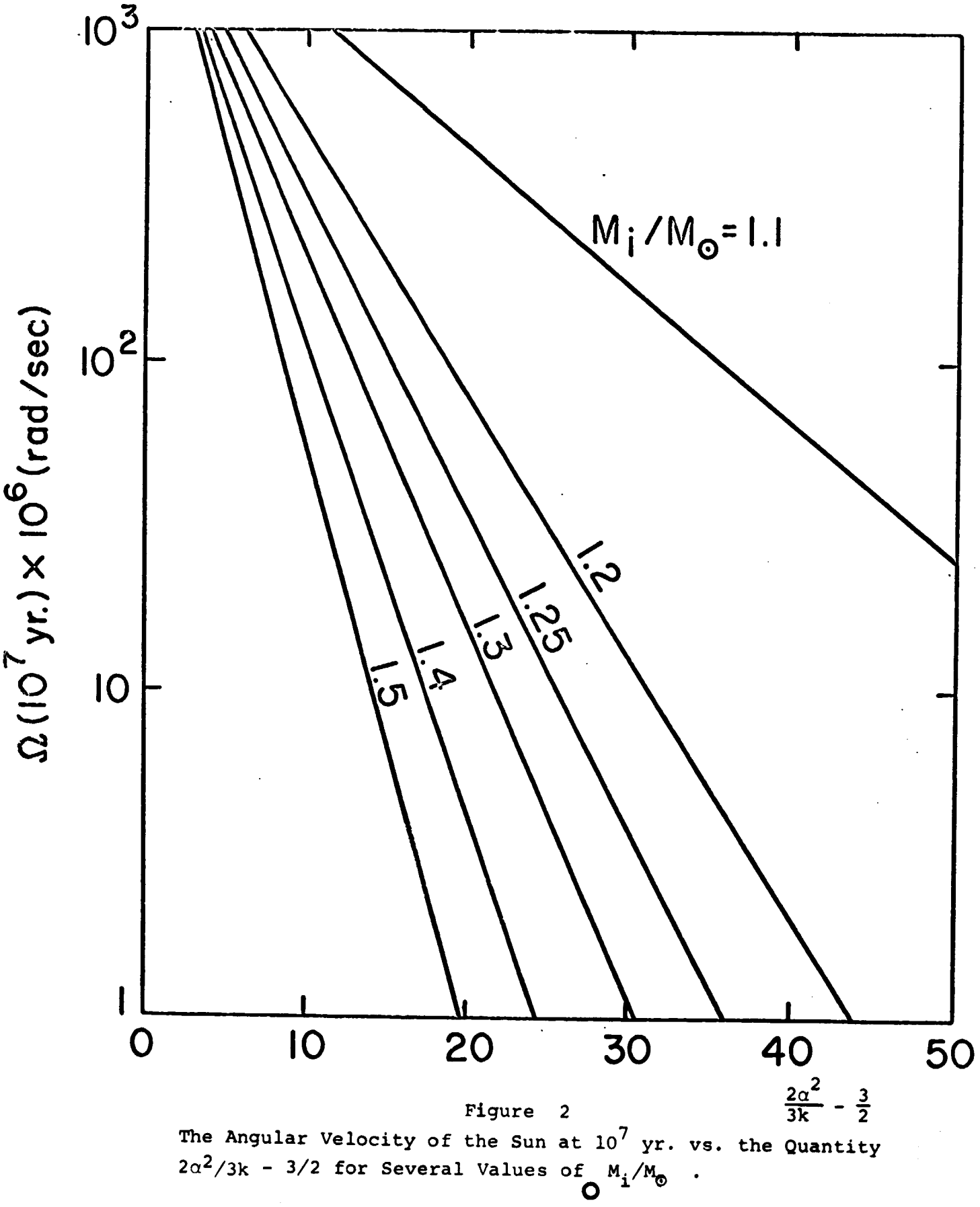

Figure 2

The Angular Velocity of the Sun at 10^7 yr. vs. the Quantity $2\alpha^2/3k - 3/2$ for Several Values of $M_i/M_\odot$.

2.3 A Simple Despin Model

In the previous two sections, the model solar environment used in the original T Tauri heating calculations and then some general observations on the solar spin decay were presented. The spin decay history is of great importance because of the intimate connection between the angular velocity, solar magnetic field, and the $|V \times B|$ unipolar driving field. It has been shown (Sonett et al 1969) that small changes in the time constant for the magnetic field when used with the Modisette despin theory produce a drastic reduction in the unipolar driving field and total unipolar heating. In this section a simple class of T Tauri solar environments will be examined. The adjective "simple" refers to the method by which the models are obtained. The basic equation is the integrated form of the angular momentum conservation equation, Equation (27), where the quantities α and k were assumed to be constants throughout the solar contraction. The second assumption is a given time dependence for the solar mass. An average value from the data presented by Kuhi (1964) together with a total mass loss of $.25M_{\odot}$ is assumed

$$M(t) = M_{\odot}(1 + .25e^{-5.6 \times 10^{-7}t}) \qquad (29)$$

where the time is given in years. The solar mass and mass loss rate are shown in Figure 3. From the data presented by Iben (1965) an empirical expression for the maximum contraction rate for the solar radius was obtained:

$$\frac{R(t)}{R_\odot} = 51(1 + t)^{-.195} - 1 \qquad (30)$$

where t is in years.

The value obtained from this expression was then compared with the value obtained from equation (27) on the assumption that the contraction history is moving along a track which maintains the angular velocity at the break up value:

$$R_c(t) = R_i(M(t)/M_i)^{2\delta-1} \qquad (31)$$

where $\delta = \frac{2\alpha^2}{3k} - 1$. Notice that $R_c(t)$ depends only on the time history of the solar mass and the parameters α and k . If the value of R obtained from equation (30) is less than the value of R_c from equation (31), the solar radius is set equal to R_c . From equation (27) it can be seen that the angular velocity increases as $R(t)$ decreases. Therefore, if $R(t) < R_c(t)$, the

Figure 3 - $\frac{\Delta M}{M_\odot}$ and $\frac{dM}{dt}$ as Function of Time

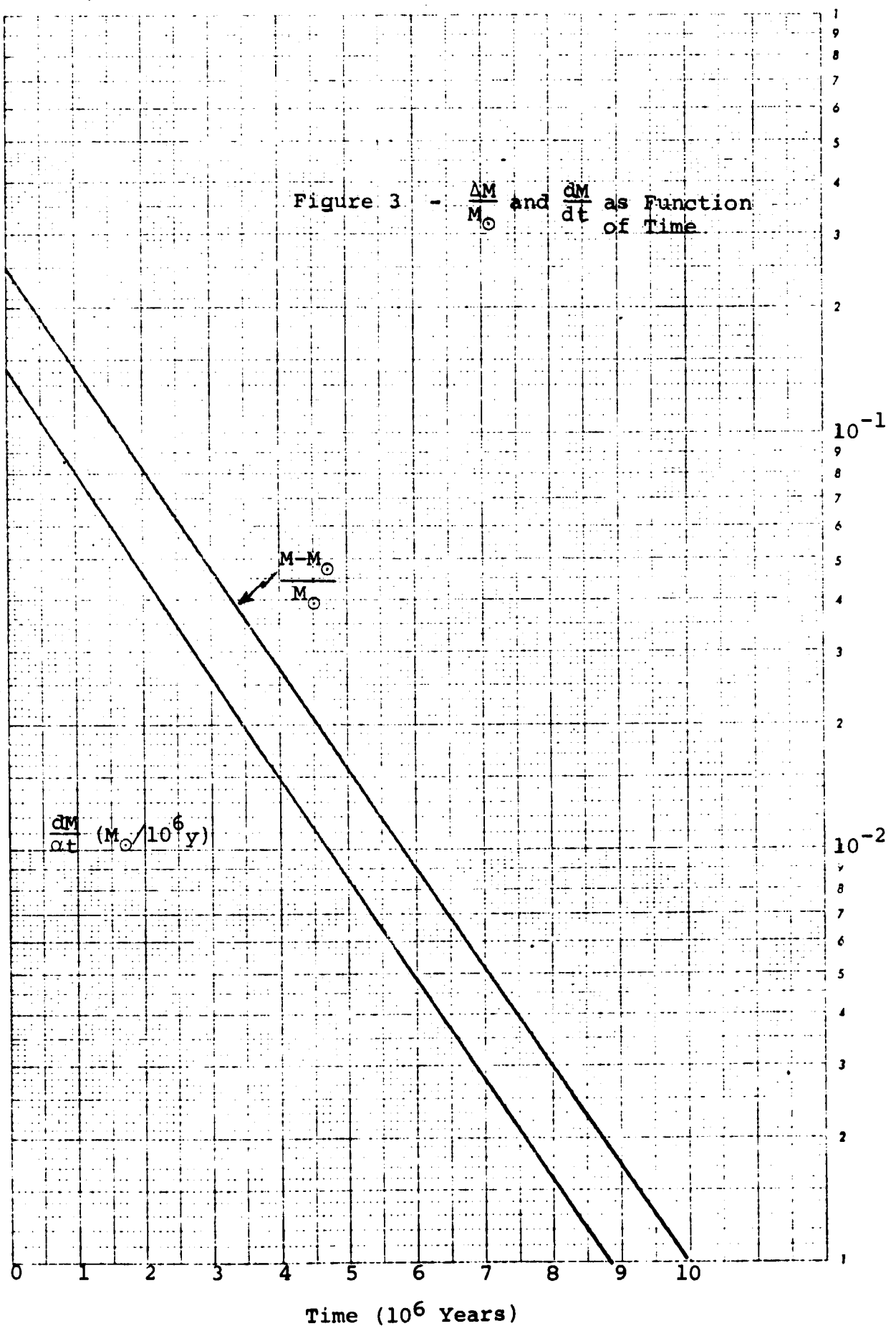

critical spin rate would be exceeded. In Figure 4, three examples are shown for the solar radius as a function of time. In all three, α is equal to 1.4. For $k = .134$, a fully convective sun, the radius never reaches the value predicted by equation (30). The entire history to $t = 12 \times 10^6$ years follows a critical spin condition. With smaller values of k and, hence, denser solar cores, the radius follows the value of R_c for some period of time and then switches to the value predicted by equation (30). Note that δ increases as α increases and k decreases. As δ increases, the effective angular momentum loss also increases bringing the angular spin rate below the critical value. This is shown clearly in Figure 5. In all but the case for $k = .134$ there is a sharp break at the time when the angular momentum loss is finally sufficient to decrease the spin rate below the critical value. Because the T Tauri mass loss rate effectively ends before the contraction given by equation (30) is complete, the three cases which do not follow the critical path show a late time increase in the spin rate.

The maximum value of the solar magnetic field can be obtained by combining equations (10) and (11) and noting that

$$\frac{dM}{dt} = -4\pi m_p V_A R_A^2 \quad . \qquad (32)$$

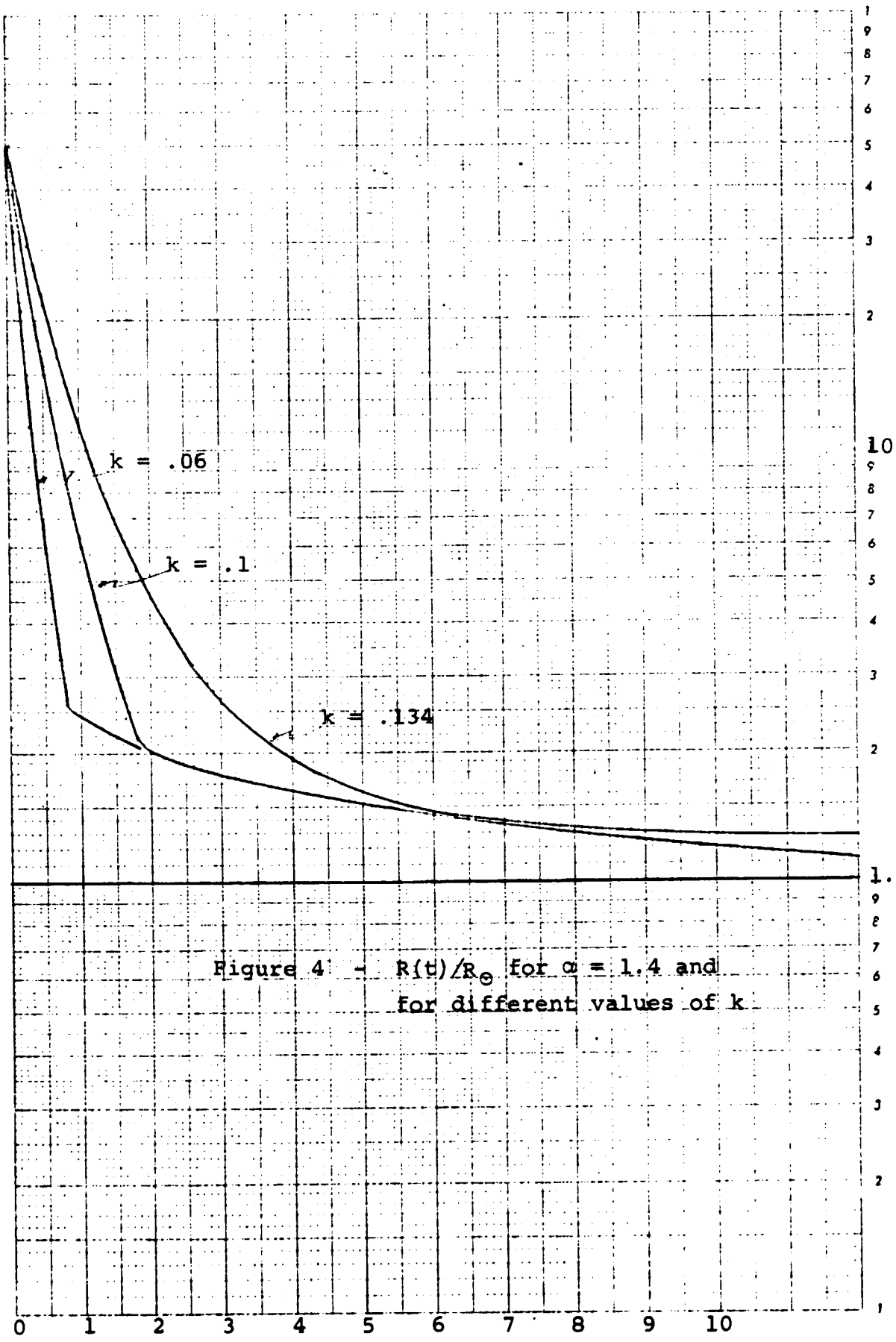

Figure 4 - $R(t)/R_\odot$ for $\alpha = 1.4$ and for different values of k

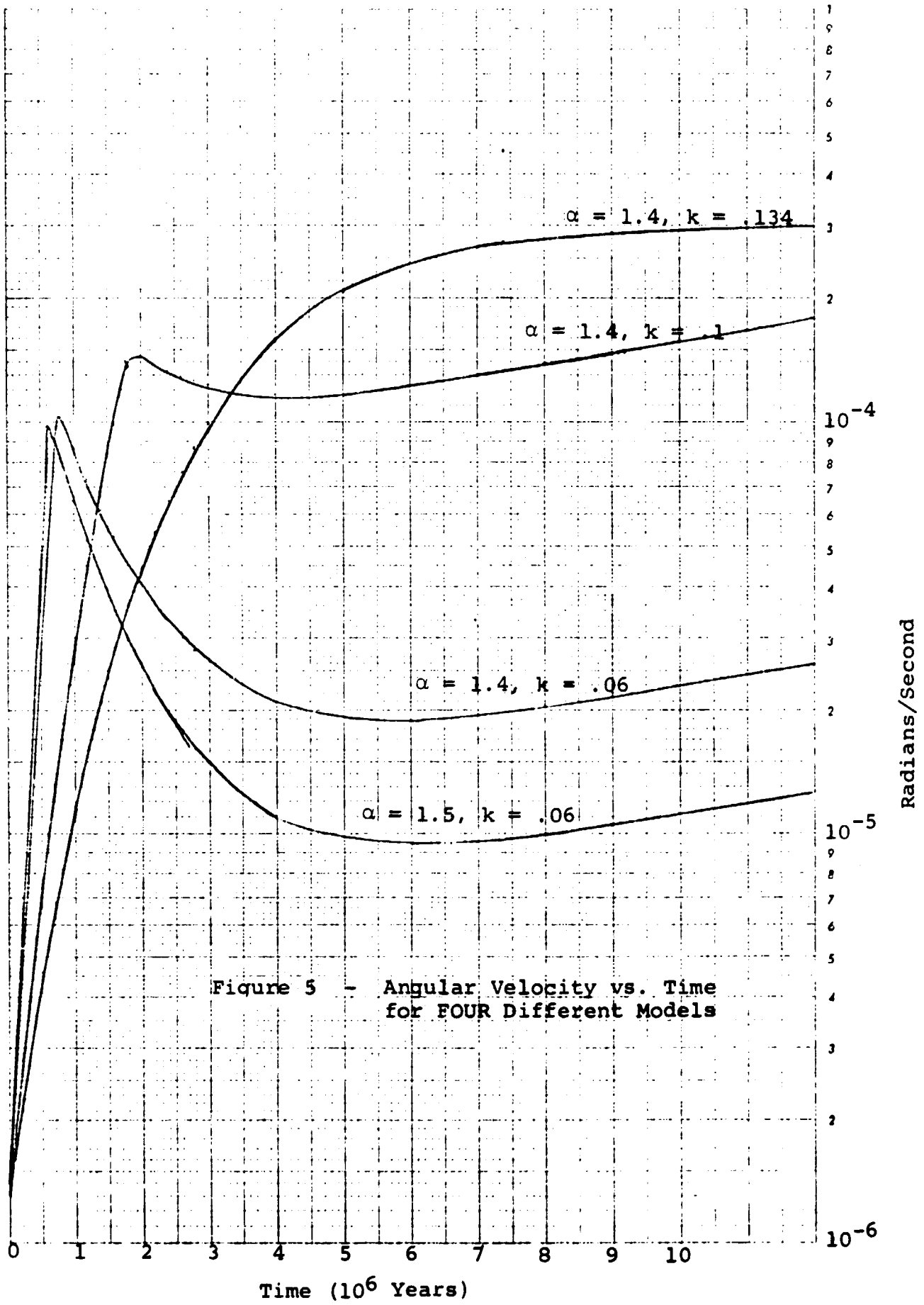

Figure 5 - Angular Velocity vs. Time for FOUR Different Models

One obtains

$$\left(B_s\right)_{max} = B_s = 1.14 \times 10^{-5} \alpha (R_\odot / R(t)) \sqrt{V_A \frac{dM}{dt}} \text{ gauss} \tag{33}$$

where dM/dt is in units of $10^{-7} M_\odot$/year and V_A is in meters/second. The value of the escape velocity at the solar surface has been used for V_A :

$$V_A = 6.19 \times 10^5 \sqrt{\frac{MR_\odot}{M_\odot R}} \text{ m/second} \tag{34}$$

The maximum value for V_A is 6.19×10^5 m/s at the end of the contraction and T Tauri mass loss. At the beginning of the contraction, V_A is much smaller. In any case, V_A is always less than the post coronal expansion velocity of 1.2×10^5 m/s during T Tauri phase. The results of the calculation for the magnetic field at the coronal base are shown in Figure 6 for four cases. Note that the coronal base magnetic field increases in magnitude from case to case as α increases. For the model discussed in Section 2.1, the maximum magnetic field is a constant 24 gauss over this time period.

The important quantity from the viewpoint of the unipolar generator is the V x B driving field. For the four cases, this driving field is shown in

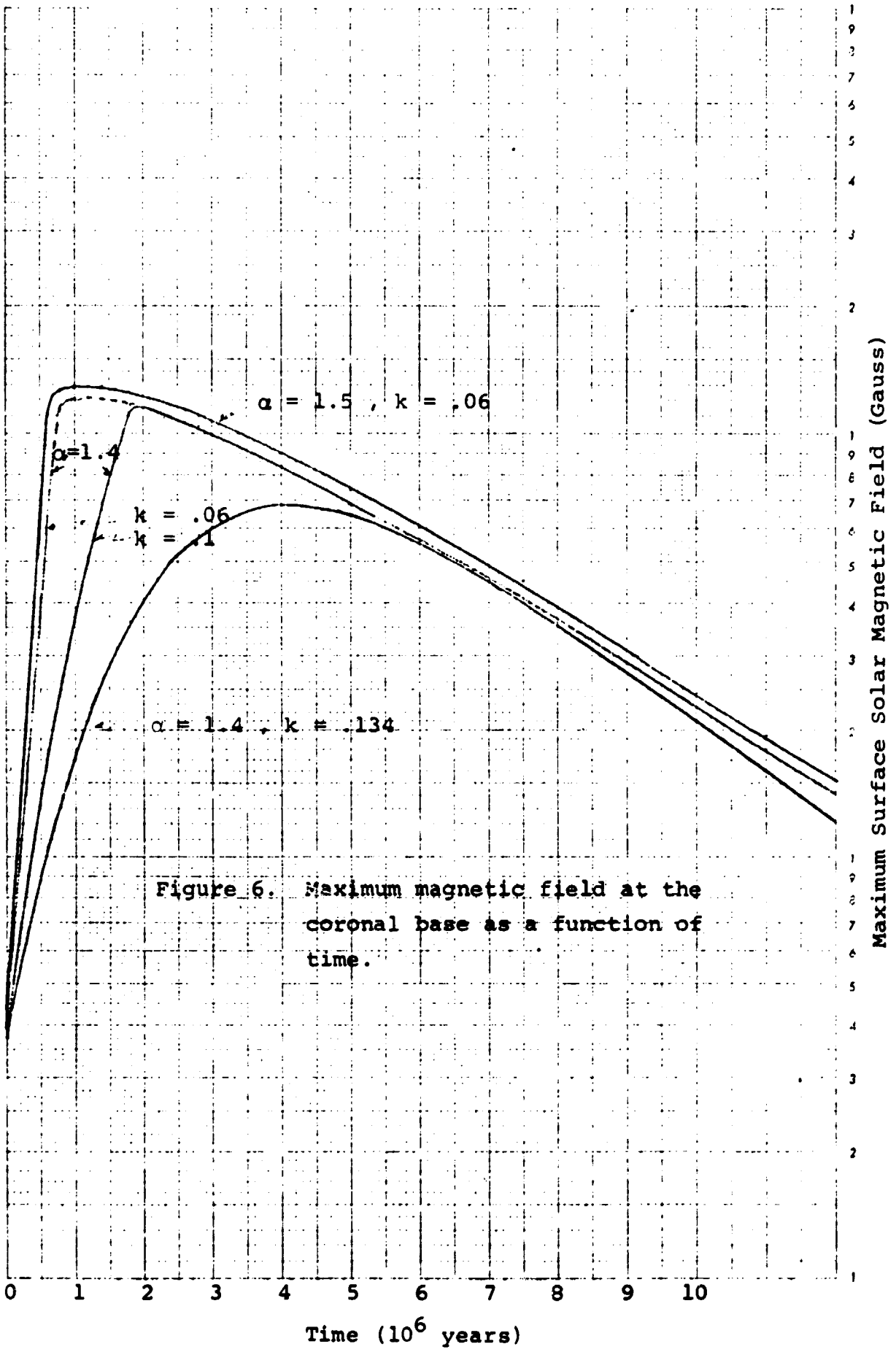

Figure 6. Maximum magnetic field at the coronal base as a function of time.

Figure 7. The field begins at a value of approximately 5 volts/meter and rapidly rises, especially for those cases which break away from the critical spin rate. During the first half million years, the field can increase by as much as a factor of 7 for one of these models. In the model described in Section 2.1, the maximum unipolar driving field is 6 volts/meter at the earth's orbit, remaining approximately constant during the time period 0 - 5 million years. Thus, the models shown here tend to produce a driving field which is of the same size to 7 times greater. The concept of a higher driving field for the heating history is explored further in the next section.

The last very significant two quantities to be discussed in this section are the momentum flux (ρV^2) and the energy flux $(\frac{1}{2}\rho V^3)$ at the earth orbit. The first of these two quantities strongly affects the formation of a planetary bow shock and the cutoff or k factor as described by Sonett and Colburn (1967 and 1968). More current, and hence greater heating, can take place for larger values of the momentum flux. The energy flux sets an upper limit on the integrated joule heating which can

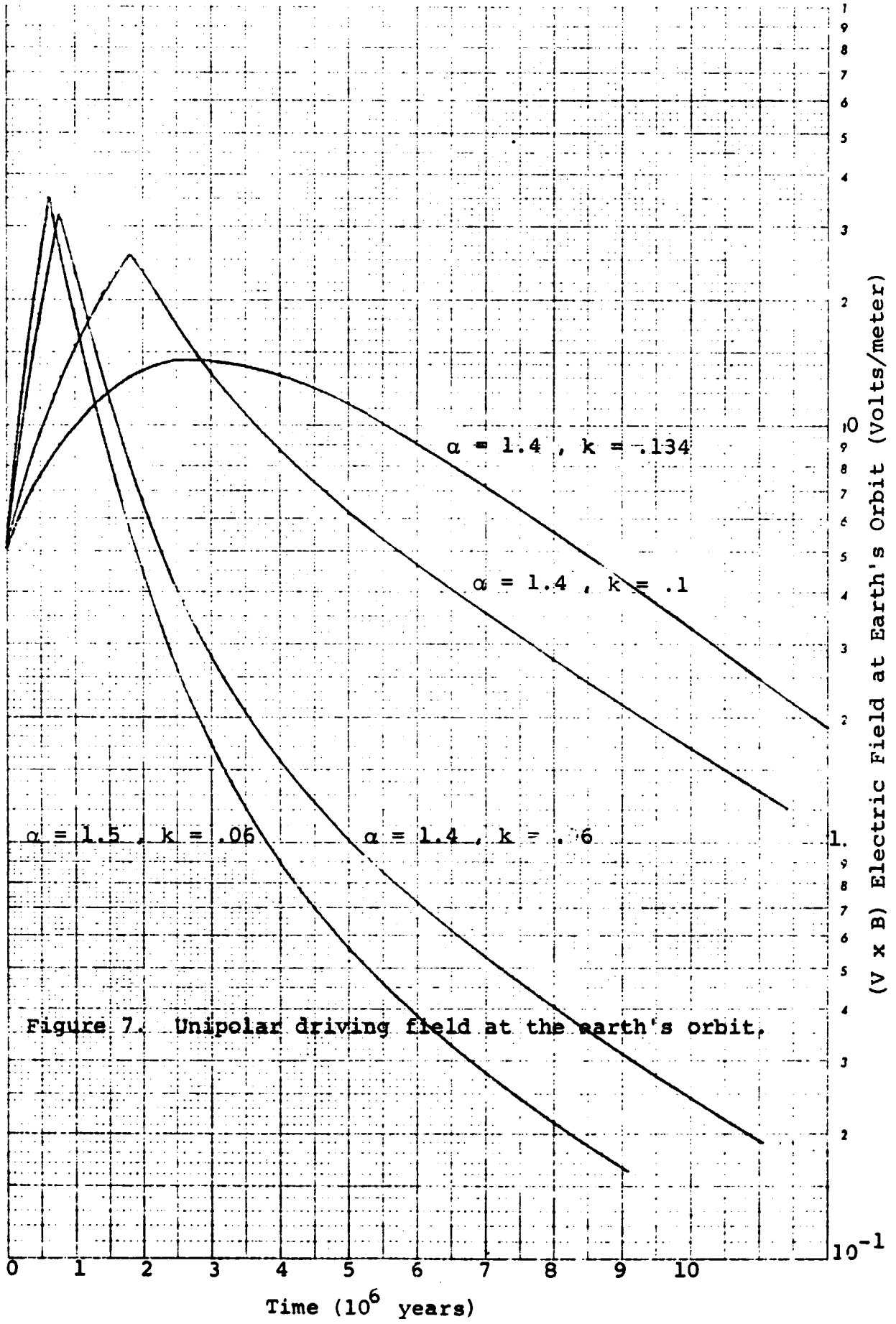

Figure 7. Unipolar driving field at the earth's orbit.

take place within a planetary body. For cases where the heating is limited by the energy flux of the solar wind, greater energy flux leads to more rapid and greater heating. The two quantities are shown in Figure 8, solid lines. Note that the velocity used in calculating these quantities is the post coronal expansion velocity of 1.2×10^6 m/s. The dashed curves are the momentum and energy flux for the original model discussed in Section 2.1. For these curves, a velocity of 2×10^5 m/s was used. However, the total mass loss was twice as great. For both models, the initial momentum flux is approximately the same at $t = 0$. However, the momentum flux for the early model decreases much more rapidly than the model of this section. This is caused by a different scale time in the mass loss rate. At 5×10^5 years, the ratio is 2, while at 10^6 years, the ratio in momentum flux is up to 3. The effect on the energy flux is even more striking. At $t = 0$, the ratio is 6. By 10^6 years, the ratio is 18. The significance of the higher energy and momentum flux will be brought out further in the next section.

Figure 8. Momentum flux and energy flux vs. time. The solid lines correspond to the model in this section with $\Delta M = .25M_\odot$. The dashed curve corresponds to the model described in Section 2.1 with $\Delta M = .5M_\odot$.

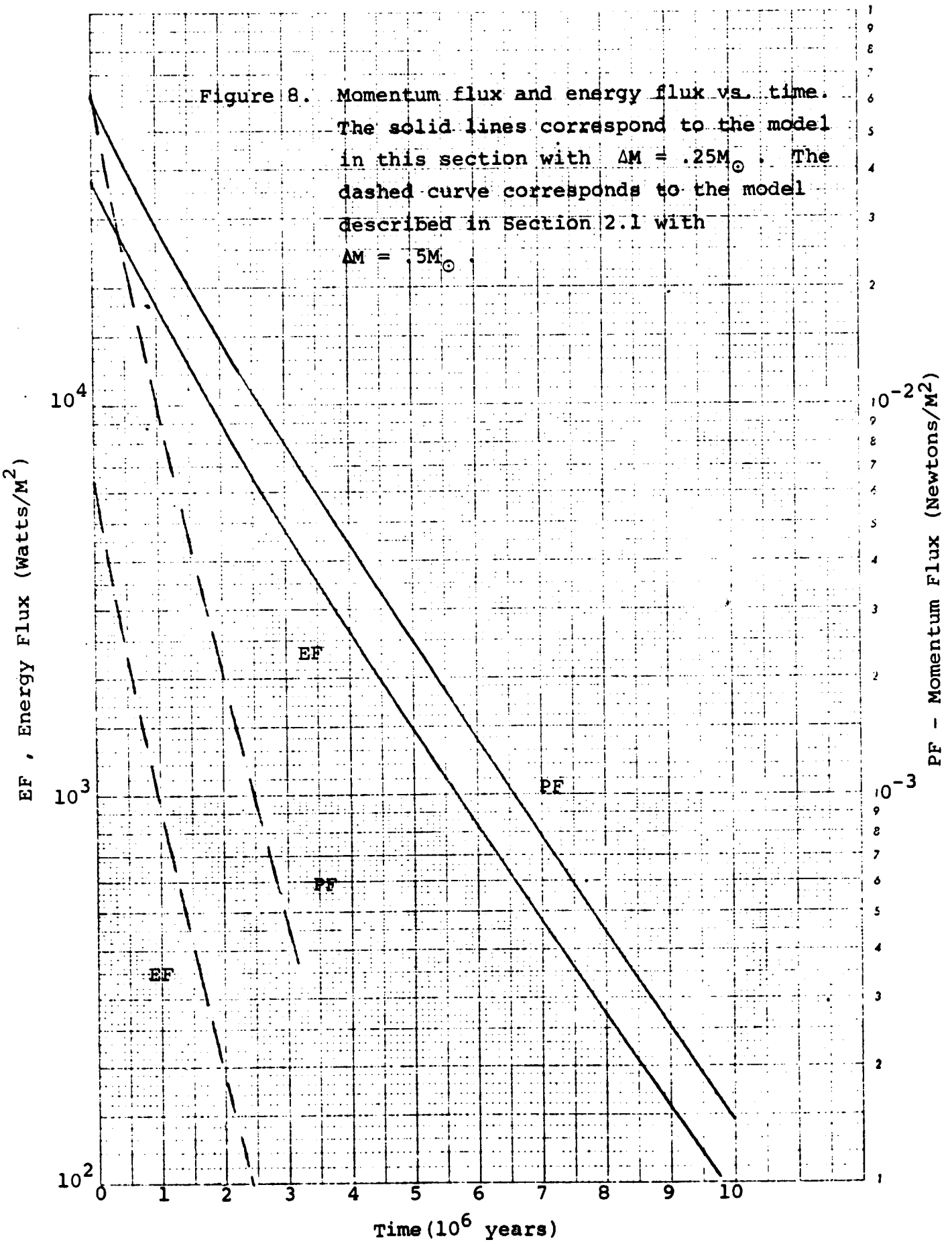

2.4 The Effect of Increased Driving Field and Decreased Circumstellar Obscuration on T Tauri Driven Unipolar Heating

One of the important assumptions associated with the T Tauri driven planetary heating by unipolar induction is the use of circumstellar obscuration to maintain the temperature of the planetary surface at a relatively high (400 to 500°C) temperature. The suggestion has been made that this assumption could be dropped if some method could be found for increasing the driving field. In the previous section, a T Tauri model was presented in which not only the driving electric field was higher than in the standard model, but the momentum and energy flux were also higher. In this section, the effect of increased driving field and also decreased hohlraum temperature will be examined starting within the framework of the original T Tauri model environment discussed in Section 2.1. It will be shown that for all cases of interest, the major heating event takes place over a period during which the parameters from the original model make up a lower limit to the set of parameters shown in Section 2.3. The planetary test body is composed of olivine (Rikitake, 1966) with an

electrical conductivity in the temperature range of interest given by:

$$\sigma = 0.01 \exp(-.5/\xi T) \text{ mhos/meter} \qquad (35)$$

where ξ is the Boltzmann constant ($\xi = 8.63 \times 10^{-5}$ electron volts/°K) and T is the temperature in degrees Kelvin. A moon sized body ($r = 1740$ kilometers) was used at a solar distance corresponding to the earth orbit. Starting hohlraum temperatures of T_{HO} of 10, 100, 200, 300, 400 and 500°C were used with a time dependence give by

$$T_H(t) = T_{HO}\, e^{-t/t_o} \qquad (36)$$

with $t_o = 8.33 \times 10^5$ years. The starting temperature for the test body was uniformly T_{HO}. Calculations were carried out to 950,000 years with the normal model E field, 10E and for extreme cases 100E and 1000E. The

thermal history of the core of the test body is shown in Figures 9 and 10. In Figure 9 all curves were obtained with the normal E field except the top most curve. For starting hohlraum temperatures of 300, 400 and 500 degrees C, the heating phase is quite rapid. The starting hohlraum temperature for each curve can be inferred from the core temperature at $t = 0$. The temperature at $t = .95 \times 10^6$ years for all three cases and for the 10E case, are within a 30° range indicating a saturation effect. As the temperature of the core increases, the conductivity increases. The total current through the test body is limited by the available momentum flux. Therefore, since the heating is proportional to I^2_{total}/σ , the heating rate in the core decreases as the conductivity increases. For $T_H = 200°C$ there is just sufficient initial heating to produce a large heating phase before the major portion of the T Tauri phase is past. For $T_H = 100°C$ or less, the unipolar heating is small, essentially negligible.

Now consider Figure 10. The heating phase for 10E and $200 \leq T_{HO} \leq 500$ is immediate. Further, the terminal core temperatures for these cases are

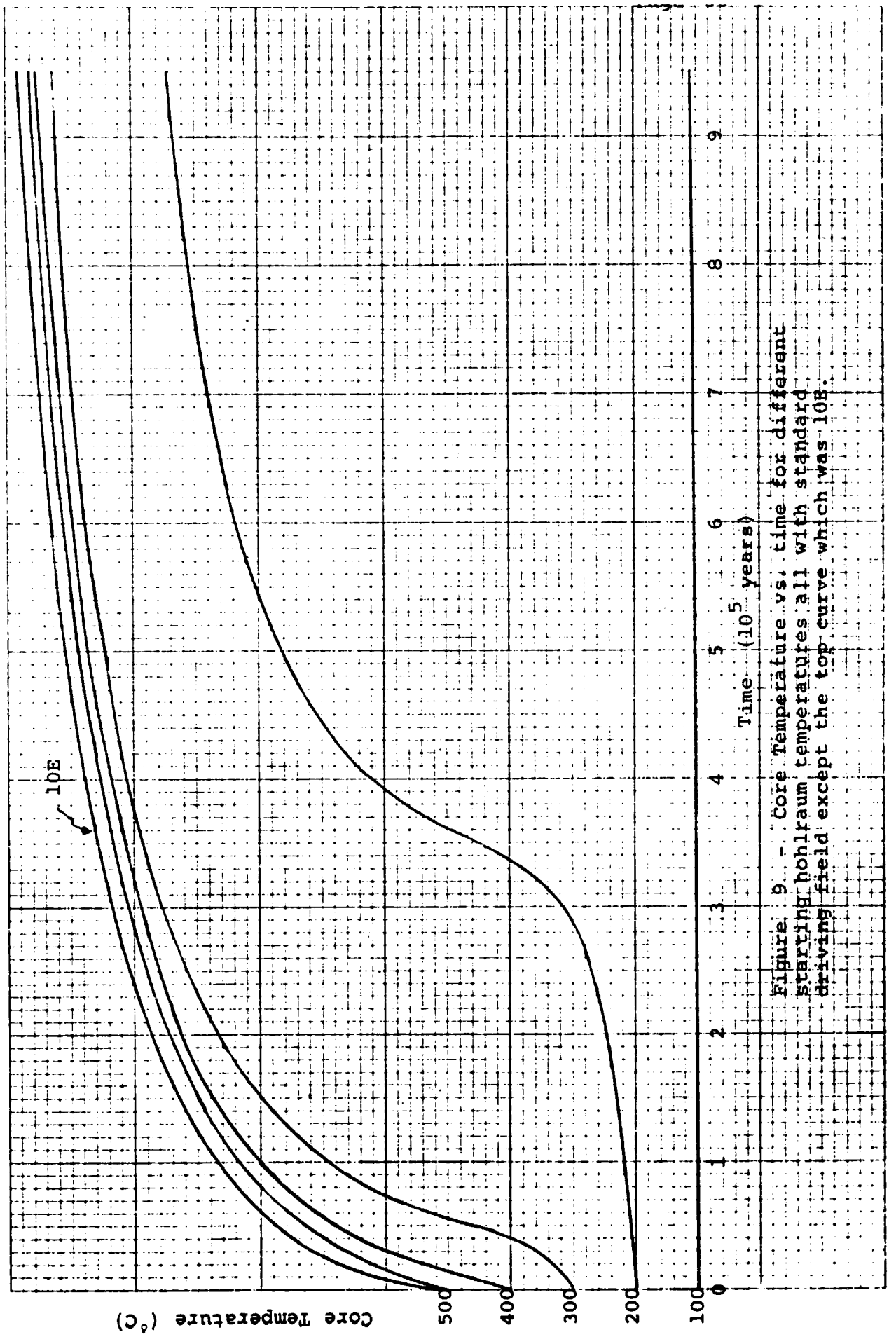

Figure 9 - Core temperature vs. time for different starting hohlraum temperatures all with standard driving field except the top curve which was 10E.

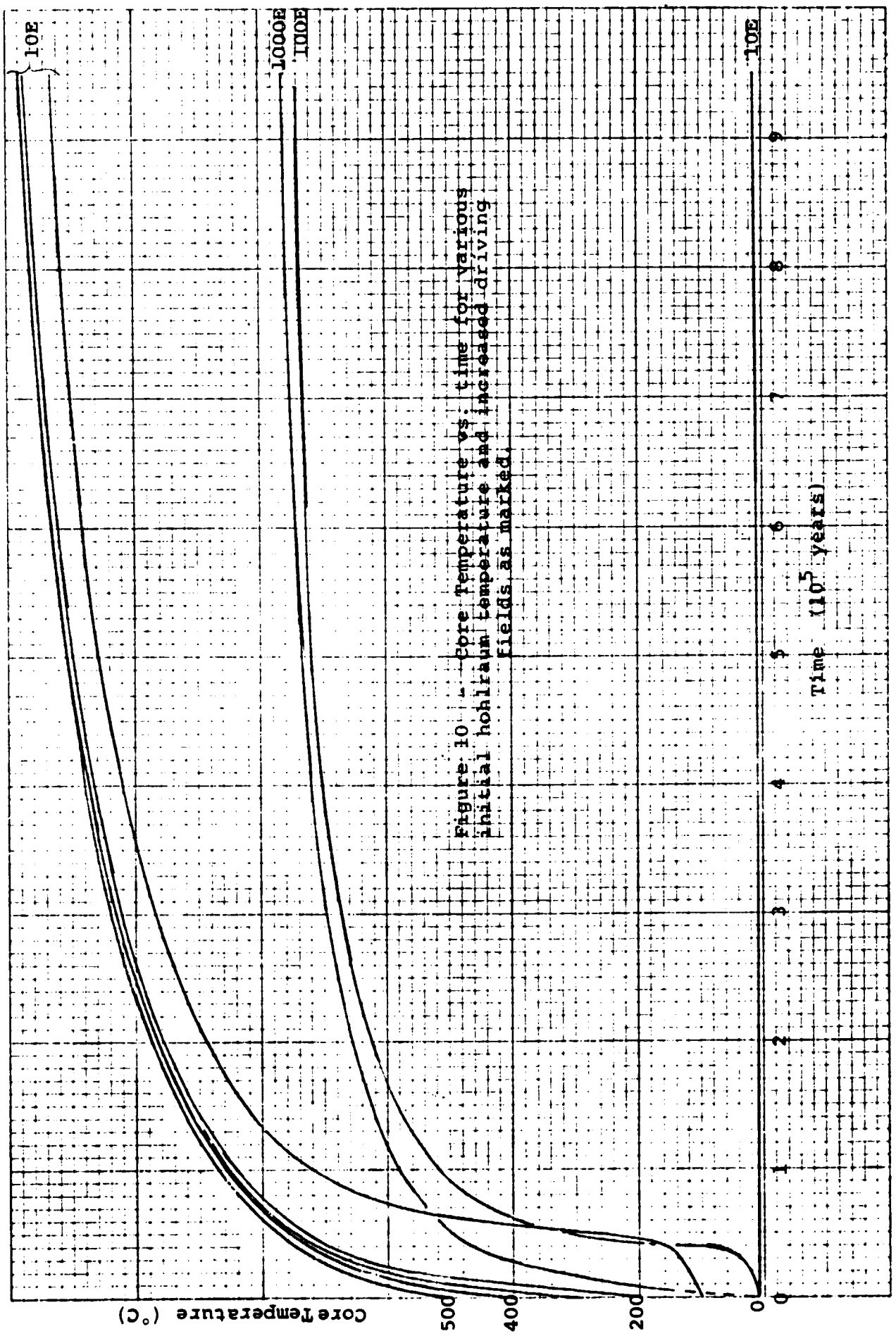

Figure 10 - Core Temperature vs. time for various initial hohlraum temperature and increased driving fields as marked.

within 10° of each other. The heating phase for T_H=100 is almost instantaneous. For a hohlraum temperature of 10°C, however, a driving field of 10E produced insignificant heating whereas 100E and 1000E produce heating which is significantly less than the higher hohlraum cases.

In order to delve deeper into the competing mechanisms of the heating process, let us examine more data for two specific initial hohlraum temperatures, 200°C and 100°C. In Figure 11, the k factor has been plotted as a function of time for these two cases. Curve 1 shows that with an enhanced field (10E) the total current is negligible until approximately 50,000 years. This corresponds to a linear core temperature increase as shown in Figure 10. The rapid increase in the k factor occurs at the same time as the rapid increase in temperature. In Figure 12, it can be seen that this rapid change in the k factor also corresponds to the time when maximum heating occurs in the core. As the k factor and core temperature continue to rise, the heating in the core decreases since the total current through the test body is being limited by the high k factor but the core conductivity is rising. Curves for

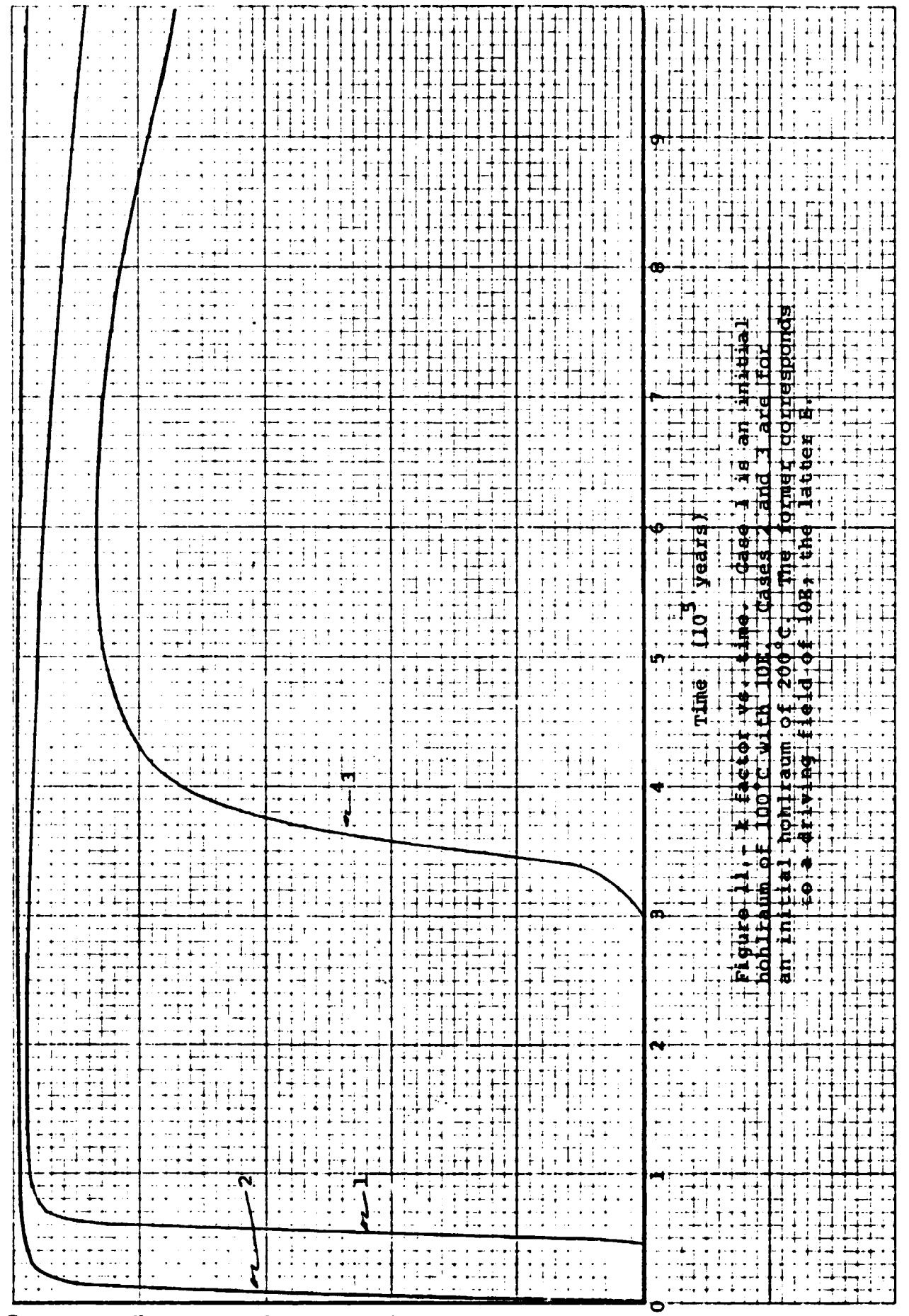

Figure 11 - k factor vs. time. Case 1 is an initial hohlraum of 100°C with 10B. Cases 2 and 3 are for an initial hohlraum of 200°C. The former corresponds to a driving field of 10B, the latter 8.

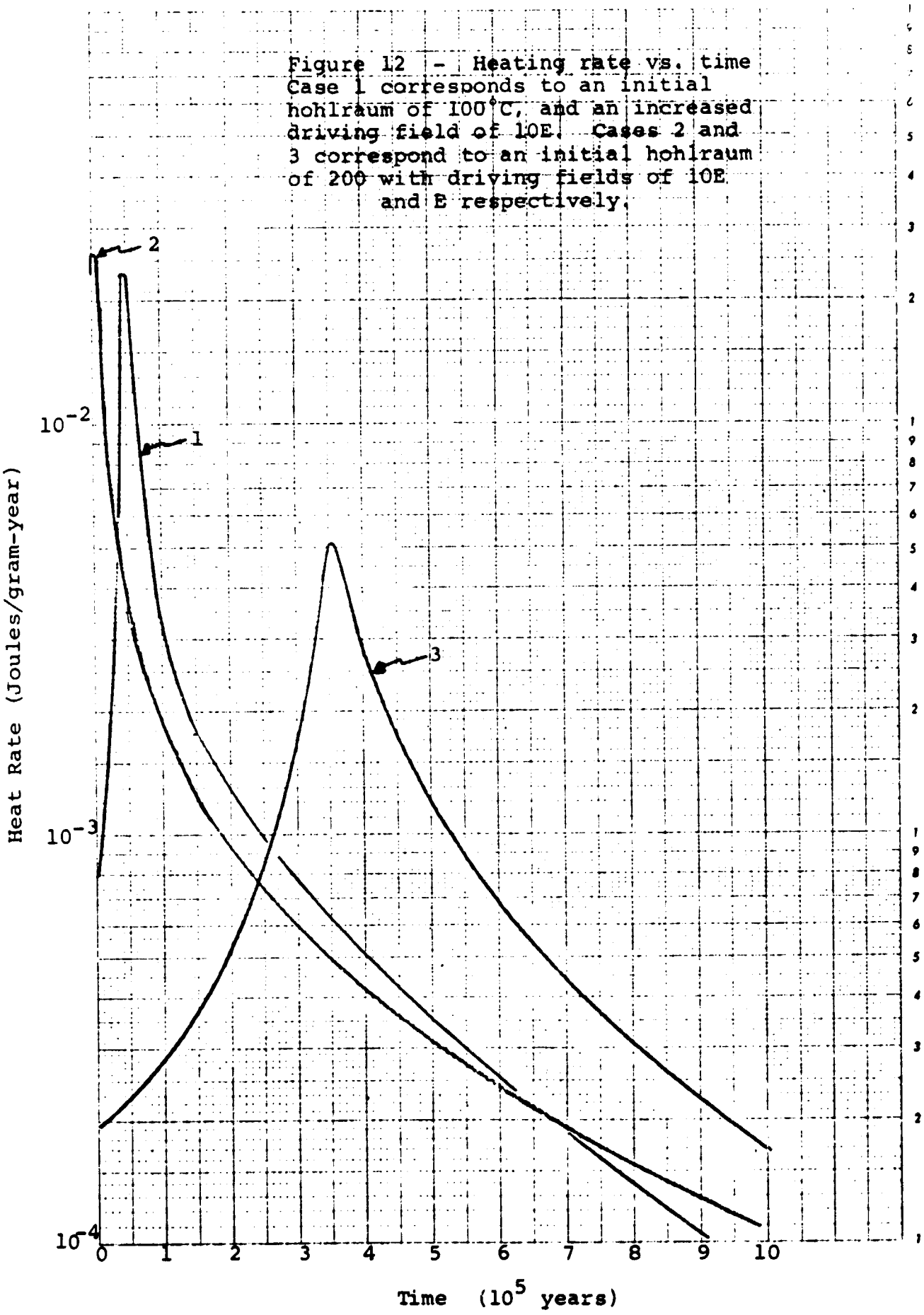

Figure 12 - Heating rate vs. time Case 1 corresponds to an initial hohlraum of 100°C, and an increased driving field of 10E. Cases 2 and 3 correspond to an initial hohlraum of 200 with driving fields of 10E and E respectively.

T_{HO} = 100 are not shown for the standard E driving field in either Figure 11 or Figure 12. The current is so small in this case that both the k factor and the joule heating are negligible. For the initial hohlraum of 200°, the sharp rise in the k factor again agrees in time with the peak in the heating curves and the greatest slope in the core temperature curve. The heating peaks occur for values of the k factor in the range .2 to .3 . For higher values of the k factor, the standoff magnetic field produced by the back current of the unipolar generator turns off the heating. From the high value of the k factor for each case where significant heating occurs, it is obvious that greater momentum flux would produce greater heating. In addition, it should be pointed out that during peak heating the models were at or very near an energy cutoff condition, i.e., the models were close to or were absorbing all of the energy incident in the solar wind. Thus, both increased momentum flux and increased energy flux would be necessary and both quantities are enhanced in the model described in Section 2.3.

interior (England et al, 1968).

The quasi-periodic sector structure of the interplanetary magnetic field necessitates consideration of the time dependent electromagnetic interaction problem. The relative motion of the moon with respect to spatial irregularities in the incident interplanetary magnetic field produces time dependent electric and magnetic field fluctuations in the lunar interior. Schwartz and Schubert (1969) modeled this time dependent interaction by the relative motion of the moon and a spatially periodic magnetic field $\underline{a}_y H_0 \exp(i2\pi z/\lambda)$, where H_0 is the amplitude and λ is the wavelength of the magnetic field oscillation and $\underline{a}_y$ is a unit vector in the y-direction. The moon moves with speed v in the negative z-direction and a coordinate system fixed in the moon is employed. The solar wind plasma is characterized by a magnetic permeability μ and an infinite electrical conductivity, while the moon is assumed to be homogeneous with constant conductivity σ and magnetic permeability μ. In the moving coordinate system, the magnetic and electric fields in the plasma are given by the real parts of

$$\underline{a}_y H_0 \exp\left[i \frac{2\pi}{\lambda} (z-vt)\right] \quad \text{and} \quad \underline{a}_x \mu v H_0 \exp\left[i \frac{2\pi}{\lambda} (z-vt)\right]$$

respectively, where $\underline{a}_x$ is a unit vector in the x-direction and z is now a coordinate in the moving reference frame.

The formulation of the electromagnetic boundary value problem requires consideration of both the oscillatory magnetic field and the oscillatory motional electric field. The lunar electromagnetic fields are determined by solving Maxwell's equations subject to the conditions that at the surface of the moon the normal component of the magnetic field and the tangential component of the electric field are continuous.

The time dependent lunar fields are forced by both the oscillatory magnetic field and the oscillatory motional electric field in the solar wind plasma. In the low frequency limit -- i.e., for length scales of the interplanetary magnetic field irregularities much larger than the moon's radius and for the time scale of the sector structure reversal large compared with the Cowling diffusion time -- the magnetic field fluctuations in the lunar interior are the sum of the variations in the driving interplanetary magnetic field plus induced magnetic field fluctuations whose magnitude is proportional to the product of the lunar magnetic Reynolds number and the magnitude of the interplanetary magnetic field fluctuations. This induced field is toroidal about an axis in the direction of the forcing motional electric field. The low frequency limit of the time dependent solution is in

agreement with the steady state unipolar induction generator solution.

This section follows closely the results of Schwartz and Schubert (1969) for a radially homogeneous moon and the extension of these results to a radially inhomogeneous moon by Schubert & Schwartz (1969). The two layer electrical conductivity model is adopted as being representative of a lunar conductivity profile that may vary from high values of conductivity in the interior to relatively low values of conductivity near the lunar surface. Blank and Sill (1969a) have described the interaction of a two layered moon and the rotating sector structure of the interplanetary magnetic field by a model that does not include the time dependent motional electric field in the solar wind. Instead, they have determined the lunar magnetic field by demanding, a priori, that the lunar magnetic field be confined to meridional planes passing through an axis parallel to the external magnetic field. This is an incorrect statement of the boundary value problem. (Blank and Sill (1969b) have now included the effect of the VXB term but their approach is justified only at the lowest frequencies). The lunar magnetic field is not confined to these meridional planes because of the magnetic field fluctuations forced by the motional electric field. It will be shown that the induced

lunar magnetic field has a toroidal component (about the direction of the motional electric field) that is precisely the induced magnetic field of the steady state induction generator solution (aside from $e^{-\omega t}$) . Fuller and Ward (1969) have considered a multi-layered lunar conductivity profile and have determined the induced lunar dipolar magnetic field and several higher modes of the "magnetic type". In their solution, they did not consider the significant induced magnetic field forced by the oscillatory motional electric field.

The major results of the present investigation can be summarized as follows. For the two layer lunar conductivity model and an infinitely conducting plasma, we determine the general solution of the time dependent electromagnetic boundary value problem. The general solution can be simplified considerably by noting that (1) the wavelength of the quasi-periodic sector structure is much larger than the radius of the moon and (2) the time scale for the field reversals of the corotating sector structure is much larger than the Cowling diffusion time through a moon whose conductivity is everywhere given by the shell conductivity. With these approximations, the magnetic field in the shell is the sum of an oscillating uniform field, parallel to the direction of the interplanetary magnetic field, an oscil-

lating dipole field whose axis is parallel to the interplanetary magnetic field, and an oscillating field which is toroidal about the axis of the motional electric field. In general, all of these contributions are of equal importance. For sufficiently low frequencies, only the uniform field and the toroidal field contribute to the magnetic field in the shell. The DC limit of the solution is in agreement with the induction generator solution for the steady state interaction of a moon moving with constant speed through a uniform magnetic field.

The solution provides sufficient physical insight to begin an interpretation of lunar surface magnetometer data. To lowest order in the approximations considered here, the solutions may be used to construct lunar conductivity models for quantitative comparison with the measured power spectra. Such conductivity models will provide information on the temperature of the lunar interior.

3.1 Theoretical Description of the Model

The approach used in this section follows the discussions of Schwartz and Schubert (1969), and Schubert and Schwartz (1969). The magnetic and electric fields in the plasma are:

$$\underline{a}_y H_o \exp\left[i\left(\frac{2\pi z}{\lambda} - \omega t\right)\right] \quad \text{and} \quad \underline{a}_x \mu v H_o \exp\left[i\left(\frac{2\pi z}{\lambda} - \omega t\right)\right],$$

respectively, where $\mu v H_o = E_m$ is the amplitude of the motional electric field oscillation and $\omega = 2\pi v/\lambda$. The two layer lunar electrical conductivity profile consists of a core of radius R_c with constant conductivity σ_c surrounded by a shell of thickness $a-R_c$ with constant conductivity σ_s (Figure13). The electromagnetic field in the plasma forces the response $\underline{E}_s\, e^{-i\omega t}$, $\underline{H}_s\, e^{-i\omega t}$ in the shell and $\underline{E}_c\, e^{-i\omega t}$, $\underline{H}_c\, e^{-i\omega t}$ in the core. The magnetic field in the lunar interior satisfies the vector Helmholtz equation

$$\nabla^2 \underline{H}_{s,c} + k_{s,c}^2 \underline{H}_{s,c} = 0 \qquad (37)$$

where ∇^2 is the Laplacian operator,

$$k_{s,c}^2 = \mu\epsilon\, \omega^2 + i\sigma_{s,c}\mu\omega \qquad (38)$$

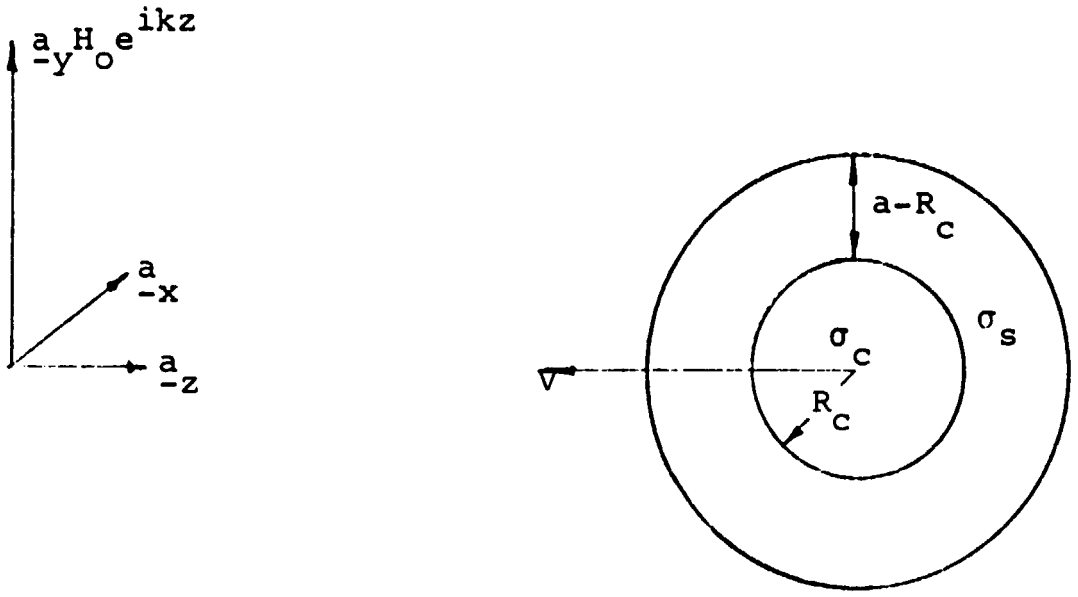

(a)

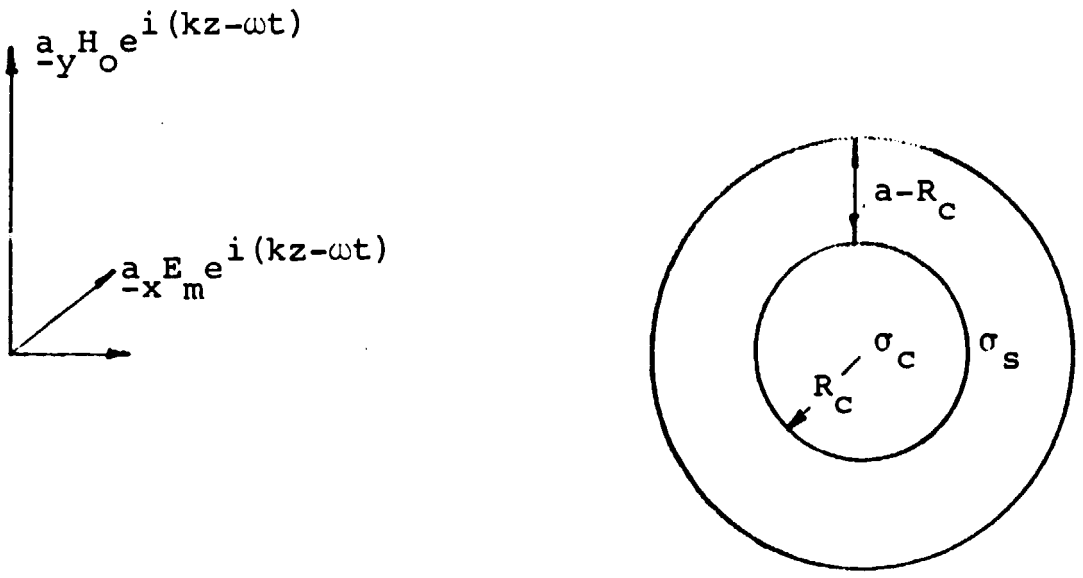

(b)

FIGURE 13

(a) Moon with two layer conductivity profile moving with speed v relative to a spatially periodic magnetic field and

(b) The relative motion viewed by an observer co-moving with the moon. A traveling electromagnetic wave appears incident on the moon.

and ϵ is the lunar permittivity. The electric fields $\underline{E}_{s,c}$ are determined from Ampere's law. The boundary conditions are the continuity of the tangential component of the electric field at r = a and r = R_c (r,θ,φ are spherical polar coordinates) and the continuity of the tangential component of the magnetic field at r = R_c. This model approximates the current layer in the plasma by a sheet of surface current whose strength is determined by the magnitude of the discontinuity in the tangential component of the magnetic field at r = a. Discussions of the current sheet approximation have been given by Johnson and Midgley (1968) and Blank and Sill (1969a).

The solution to this problem is easily obtained with the aid of Stratton (1941). The spherical harmonic expansions of the forcing fields are

$$\underline{H} = - H_0 e^{-i\omega t} \sum_{n=1}^{\infty} \beta_n (\underline{m}_{e1n}^{(1)} + i\, \underline{n}_{01n}^{(1)}) \qquad (39)$$

$$\underline{E} = E_m e^{-i\omega t} \sum_{n=1}^{\infty} \beta_n (\underline{m}_{01n}^{(1)} - i\, \underline{n}_{e1n}^{(1)}) \qquad (40)$$

where

$$\beta_n = \frac{i^n (2n+1)}{n(n+1)} \qquad (41)$$

$$\underset{\substack{o\\e}}{\underline{m}}^{(1)}_{1n} = j_n(kr)\left\{\pm \frac{P_n^1(\cos\theta)}{\sin\theta}\begin{Bmatrix}\cos\\ \sin\end{Bmatrix}\varphi\ \hat{\underline{\theta}} - \frac{dP_n^1(\cos\theta)}{d\theta}\begin{Bmatrix}\sin\\ \cos\end{Bmatrix}\varphi\ \hat{\underline{\varphi}}\right\} \tag{42}$$

$$\underset{\substack{o\\e}}{\underline{n}}^{(1)}_{1n} = \frac{n(n+1)}{kr} j_n(kr) P_n^1(\cos\theta)\begin{Bmatrix}\sin\\ \cos\end{Bmatrix}\varphi\ \hat{\underline{r}} + \frac{1}{kr}\frac{d}{dr}\left\{rj_n\left(\frac{2\pi r}{\lambda}\right)\right\}\left\{\frac{d}{d\theta}P_n^1(\cos\theta)\begin{Bmatrix}\sin\\ \cos\end{Bmatrix}\varphi\ \hat{\underline{\theta}} \pm \frac{P_n^1(\cos\theta)}{\sin\theta}\begin{Bmatrix}\cos\\ \sin\end{Bmatrix}\varphi\ \hat{\underline{\varphi}}\right\} \tag{43}$$

where $k = 2\pi/\lambda = \omega/v$. The spherical Bessel functions j_n and the associated Legendre functions $P_n^1(\cos\theta)$ are defined as in Stratton (1941). The vectors $\hat{r},\hat{\theta},\hat{\varphi}$ are the orthogonal unit vectors of the spherical polar coordinate system.

The electric and magnetic fields inside the core are

$$\underline{E}_c = E_m \sum_{n=1}^{\infty} \beta_n \left| a_n^c\ \underline{m}_{1n}^{(1)c} - i\ b_n^c\ \underline{n}_{1n}^{(1)c} \right| \tag{44}$$

$$\underline{H}_c = \frac{vk_c H_0}{\omega} \sum_{n=1}^{\infty} \beta_n \left| b_n^c\ \underline{m}_{1n}^{(1)c} + i\ a_n^c\ \underline{n}_{1n}^{(1)c} \right| \tag{45}$$

where $\underset{\substack{o\\e}}{\underline{m}}^{(1)c}_{1n}$ and $\underset{\substack{o\\e}}{\underline{n}}^{(1)c}_{1n}$ are obtained from Eqs. (42) and

(43) by replacing k with k_c. Similarly, within the shell the fields are

$$\underline{E}_s = E_m \sum_{n=1}^{\infty} \beta_n \left(a_n^{(1)s} \underline{m}_{o1n}^{(1)s} - i\, b_n^{(1)s} \underline{n}_{e1n}^{(1)s} + a_n^{(3)s} \underline{m}_{o1n}^{(3)s} - i\, b_n^{(3)s} \underline{n}_{e1n}^{(3)s} \right) \tag{46}$$

$$\underline{H}_s = - \frac{v k_s H_0}{\omega} \sum_{n=1}^{\infty} \beta_n \left(b_n^{(1)s} \underline{m}_{e1n}^{(1)s} + i\, a_n^{(1)s} \underline{n}_{o1n}^{(1)s} + b_n^{(3)s} \underline{m}_{e1n}^{(3)s} + i a_n^{(3)s} \underline{n}_{o1n}^{(3)s} \right) \tag{47}$$

where $\underline{m}_{e}^{(1)s}_{o1n}$ and $\underline{n}_{e}^{(1)s}_{o1n}$ are obtained from equations (42) and (43) by replacing k with k_s and $\underline{m}_{e}^{(3)s}_{o1n}$ and $\underline{n}_{o}^{(3)s}_{1n}$ are obtained from equations (42) & (43) by substituting k_s for k and also using the spherical Bessel function $h_n^{(1)}$ in place of j_n. The values of the coefficients a_n^c, b_n^c, $a_n^{(1)s}$, $a_n^{(3)s}$ and $b_n^{(3)s}$ are given in Appendix A at the end of Section 3.0.

3.2 Discussion of the Solution

To interpret the data from lunar surface magnetometer experiments we must compute the magnetic field at $r = a$ as a function of ω for particular lunar conductivity models and compare these computations with the measured power spectra. The essential dimensionless parameters on which the solution depends are $ka = 2\pi a/\lambda$, $k_s a$ and $k_c R_c$. For the interaction of the moon with the rotating sector structure of the interplanetary magnetic field ka is $0(10^{-4})$. Thus we will consider the simplification $ka \ll 1$. For the physical pheonomenon of interest it is appropriate to approximate $k^2_{s,c}$ with $i\,\sigma_{s,c}\mu\omega$. This is consistent with the low frequency approximation $ka \ll 1$. The absence of a lunar bow shock places an upper limit of 10^{-5} mhos/m on the electrical conductivity of the shell. Thus $\left|k_s^2\, a^2\right| \ll 1$ for $\omega \ll .025\ \text{sec}^{-1}$. Since ω is $0(10^{-5}\text{sec}^{-1})$ for the problem of the interaction of the moon and the rotating sector structure of the interplanetary magnetic field and since the power density spectrum of the interplanetary magnetic field (Coleman 1968) contains significant power at the frequencies associated with field reversals caused by the corotation of the field's sector structure, the frequency range $\omega \ll .025\ \text{sec}^{-1}$ represents an appropriate one for

investigation. We proceed to determine the form of the general solution under the conditions $2\pi a/\lambda \ll 1$ and $|k_s a| \ll 1$. Since $R_c \leq a$, $|k_s R_c|$ is also small compared with unity.

Since we are mainly interested in the magnetic field at r=a, we compute the coefficients $a_n^{(1)s}$, $a_n^{(3)s}$, $b_n^{(1)s}$ and $b_n^{(3)s}$ under the approximations $2\pi a/\lambda \ll 1$ and $|k_s a| \ll 1$ and find

$$a_n^{(1)s} \sim \frac{(ka)^n (k_s a)^{-n}}{\left\{1 - \left(\frac{R_c}{a}\right)^{2n+1} B_n(k_c R_c)\right\}} , \qquad (48)$$

$$a_n^{(3)s} \sim \frac{-i}{(2n+1)} \frac{1}{\left\{(2n-1)!!\right\}^2} \frac{(ka)^n (k_s a)^{n+1} \left(\frac{R_c}{a}\right)^{2n+1} B_n(k_c R_c)}{\left\{1 - \left(\frac{R_c}{a}\right)^{2n+1} B_n(k_c R_c)\right\}} , \qquad (49)$$

$$b_n^{(1)s} \frac{(ka)^{n-1} (k_s a)^{-n+1}}{\left\{1 - \left(\frac{R_c}{a}\right)^{2n+1}\right\}} , \qquad (50)$$

$$b_n^{(3)s} \sim \frac{i(n+1)}{n(2n+1)} \frac{(ka)^{n-1}(k_s a)^{n+2}}{\left\{(2n-1)!!\right\}^2} \frac{\left(\frac{R_c}{a}\right)^{2n+1}}{\left\{1 - \left(\frac{R_c}{a}\right)^{2n+1}\right\}} , \tag{51}$$

where

$$B_n(k_c R_c) = \frac{p_n(k_c R_c) - (n+1) j_n(k_c R_c)}{p_n(k_c R_c) + n\, j_n(k_c R_c)} , \tag{52}$$

and

$$(2n-1)!! = (2n-1)(2n-3)(2n-5).....1 , \tag{53}$$

We must also determine the functions $\underline{m}_{0_{e}ln}^{(1)s}$, $\underline{m}_{0_{e}ln}^{(3)s}$, $\underline{n}_{0_{e}ln}^{(1)s}$ and $\underline{n}_{0_{e}ln}^{(3)s}$ for $\frac{2\pi a}{\lambda} \ll 1$ and $|k_s a| \ll 1$.

It will be sufficient for our purpose to note that

$$\underline{m}_{0_{e}ln}^{(1)s} = 0\left((k_s a)^n \right) , \tag{54}$$

$$\underline{m}_{0_{e}ln}^{(3)s} = 0\left((k_s a)^{-n-1} \right) , \tag{55}$$

$$\underline{n}_{0_{e_{ln}}}^{(1)s} = 0\left((k_s a)^{n-1} \right) \quad , \qquad (56)$$

$$\underline{n}_{0_{e_{ln}}}^{(3)s} = 0\left((k_s a)^{-n-2} \right) \quad , \qquad (57)$$

Consider the order of magnitude of each of the terms in the expressions for $\underline{H}_s$

$$\frac{k_s}{k} b_n^{(1)s} \underline{m}_{e_{ln}}^{(1)s} = 0\left\{ (ka)^{n-2} (k_s a)^2 \right\} \quad , \qquad (58)$$

$$\frac{k_s}{k} a_n^{(1)s} \underline{n}_{0_{ln}}^{(1)s} = 0\left\{ (ka)^{n-1} \right\} \quad , \qquad (59)$$

$$\frac{k_s}{k} b_n^{(3)s} \underline{m}_{e_{ln}}^{(3)s} = 0\left\{ (ka)^{n-2} (k_s a)^2 \right\} \quad , \qquad (60)$$

$$\frac{k_s}{k} a_n^{(3)s} \underline{n}_{0_{ln}}^{(3)s} = 0\left\{ (ks)^{n-1} \right\} \quad , \qquad (61)$$

To the lowest order of approximation only the n=1 terms need be considered. Two of these terms are

$0(1)$, while the remaining two are $0\left\langle (k_s a)^2 (\frac{2\pi a}{\lambda})^{-1} \right\rangle$. The quantity $(k_s a)^2 (\frac{2\pi a}{\lambda})^{-1} = i(\sigma_s \mu v a)$, is (aside from i) the lunar magnetic Reynolds number based on the conductivity of the shell and the moon's radius. Alternatively, one may consider $\sigma_s \mu v a$ as the ratio of the Cowling diffusion time for a body of dimension a and conductivity σ_s to the time required to move the distance a at speed v. Since the absence of a lunar bow shock requires only that $\sigma_s < 10^{-5}$ mhos/m, the lunar magnetic Reynolds number is an $0(1)$ quantity, i.e. $(k_s a)^2 (\frac{2\pi a}{\lambda})^{-1}$ is $0(1)$ and consequently all the n=1 terms in the expression for $\underline{H}_s$ are of the same order. Thus we find

$$\frac{\underline{H}_s}{H_0} = \underline{a}_y \left\langle 1 - (\frac{R_c}{a})^3 B_1(k_c R_c) \right\rangle^{-1} \left\langle 1 - (\frac{R_c}{r})^3 B_1(k_c R_c) \right\rangle$$

$$+ \frac{3}{2} (\cos\theta \sin\varphi \, \hat{\underline{\theta}} + \cos\varphi \, \hat{\underline{\varphi}}) (\frac{R_c}{r})^3 B_1(k_c R_c) \left\langle 1 - (\frac{R_c}{a})^3 B_1(k_c R_c) \right\rangle^{-1}$$

$$- (\sigma_s \mu v R_c) (\sin\varphi \, \hat{\underline{\theta}} + \cos\theta \cos\varphi \, \hat{\underline{\varphi}}) \left\langle 1 - (\frac{R_c}{a})^3 \right\rangle^{-1} \left\langle \frac{r}{2R_c} + (\frac{R_c}{r})^2 \right\rangle \tag{62}$$

where

$$B_1(k_c R_c) = 1 - \frac{3}{k_c^2 R_c^2} + \frac{3 \cot k_c R_c}{k_c R_c} \tag{63}$$

Equation (62) is the major result of this section and its physical content is readily obtained. First, note that if r, α, ψ are spherical polar coordinates with the y-axis the polar axis, then

$$\cos\theta \sin\varphi \, \underline{\hat{\theta}} + \cos\varphi \, \underline{\hat{\varphi}} = - \sin\alpha \, \underline{\hat{\alpha}} \tag{64}$$

If r, γ, η are spherical polar coordinates with the x-axis the polar axis then

$$\sin\varphi \, \underline{\hat{\theta}} + \cos\theta\cos\varphi \, \underline{\hat{\varphi}} = - \sin\gamma \, \underline{\hat{n}} \tag{65}$$

The expression for the magnetic field in the lunar shell is

$$\frac{\underline{H}_s}{H_0} = \underline{a}_y \frac{\left\{1-\left(\frac{R_c}{r}\right)^3 B_1(k_c R_c)\right\}}{\left\{1-\left(\frac{R_c}{a}\right)^3 B_1(k_c R_c)\right\}} - \frac{3}{2} \sin\alpha \, \underline{\hat{\alpha}} \frac{\left(\frac{R_c}{r}\right)^3 B_1(k_c R_c)}{\left\{1-\left(\frac{R_c}{a}\right)^3 B_1(k_c R_c)\right\}}$$

$$+ (\sigma_s \mu v R_c) \sin\gamma \, \underline{\hat{n}} \frac{\left\{\frac{r}{2R_c} + \left(\frac{R_c}{r}\right)^2\right\}}{\left\{1-\left(\frac{R_c}{a}\right)^3\right\}} \tag{66}$$

The term proportional to the magnetic Reynolds number $\sigma_s \mu v R_c$ represents a magnetic field which is

toroidal about an axis in the direction of the motional electric field. This toroidal magnetic field is indentical (aside from the factor $e^{-\omega t}$) to the field of the steady state induction generator in the approximation $\sigma_s/\sigma_c \ll 1$ (see Appendix B). The contribution of the toroidal field to the total magnetic field in the shell is, to lowest order, independent of the core conductivity and the frequency (aside from $e^{-i\omega t}$). The remaining terms in the expression for $\underline{H}_s/H_0$ represent the superposition of a uniform field, in the direction of the interplanetary field, and a dipole field whose axis is parallel to the interplanetary field direction. These terms agree with the result of Blank and Sill (1969a), who pointed out that the factor $1-(\frac{R_c}{a})^3 B_1(k_c R_c)^{-1}$ represents a volume compression of the field which cannot leak into the solar wind plasma. These authors, however, failed to consider the toroidal magnetic field contribution to the total field in the linar shell. We note that the uniform and dipolar field are, to lowest order, independent of the shell conductivity. The real and imaginary parts of the function $B_1(k_c R_c)$ are shown in Figure 14.

At the lunar surface the magnetic field is

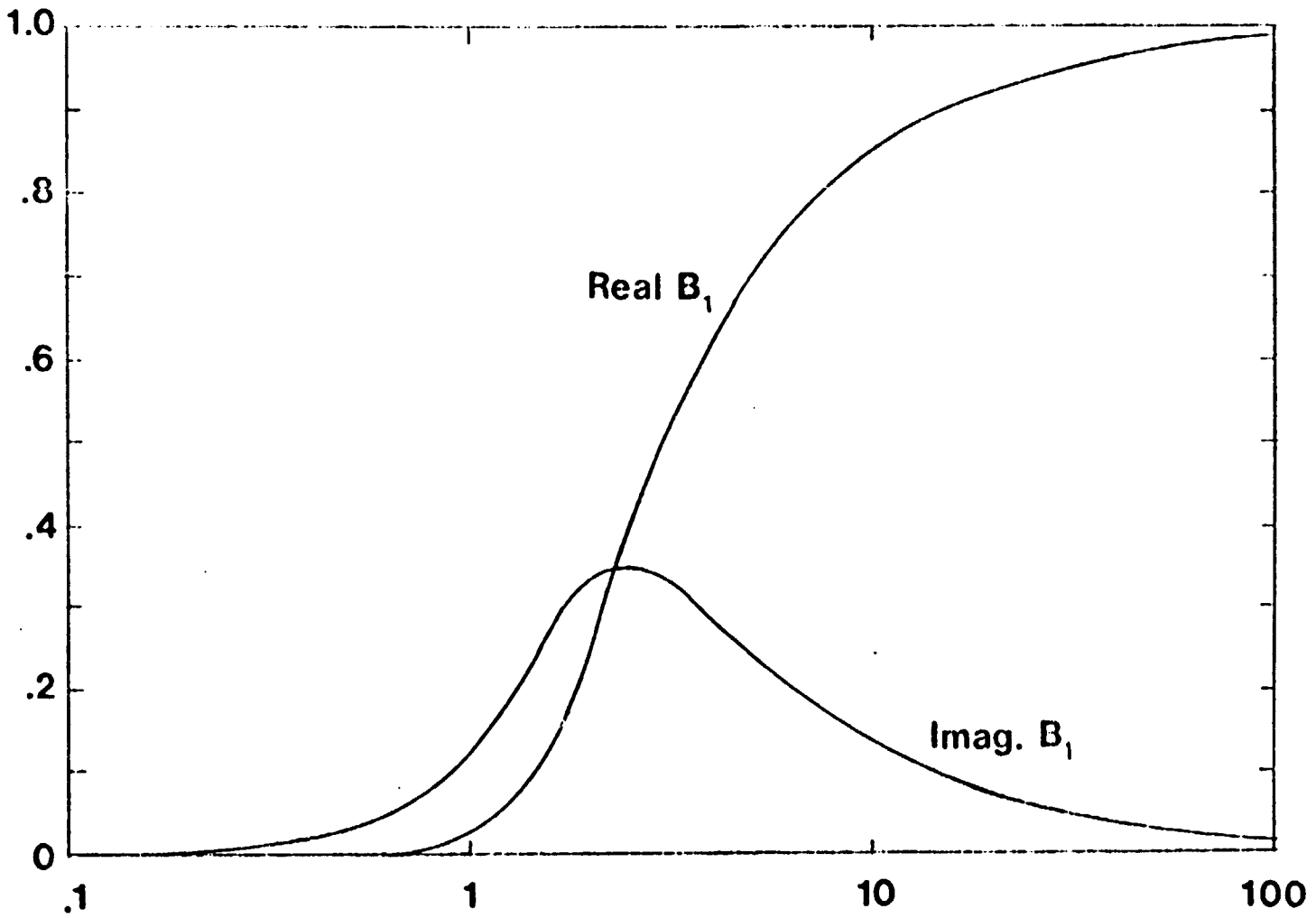

Figure 14

The real and imaginary parts of B_1 as a function of

$$\left(\frac{\sigma_c \mu \omega R_c^2}{2}\right)^{1/2}$$

$$\frac{\underline{H}_s}{H_0}\,(r=a) = \underline{a}_y + (\sigma_s \mu v a)\,\sin\gamma\,\hat{\underline{\eta}}\,\frac{(\frac{1}{2} + \frac{R_c^3}{a^3})}{(1 - \frac{R_c^3}{a^3})}$$

$$- \frac{3}{2}\sin\alpha\,\hat{\underline{\alpha}}\,\frac{(\frac{R_c}{a})^3 B_1(k_c R_c)}{\left\{1-(\frac{R_c}{a})^3 B_1(k_c R_c)\right\}} \qquad (67)$$

If the core is sufficiently conducting that $|k_c R_c| >> 1$ for $\omega = 0(10^{-5}\,\text{sec}^{-1})$ and $R_c = 0(10^6\,\text{m})$, $\sigma_c >> 10^{-1}\,\text{mhos/m})$, $B_1(k_c R_c) \approx 1$ and the surface magnetic field becomes

$$\frac{\underline{H}_s}{H_0}\,(r=a) \xrightarrow[|k_c R_c| \to \infty]{} \underline{a}_y + (\sigma_s \mu v a)\sin\gamma\,\hat{\underline{\eta}}\,\frac{(\frac{1}{2} + \frac{R_c^3}{a^3})}{(1 - \frac{R_c^3}{a^3})}$$

$$- \frac{3}{2}\sin\alpha\,\hat{\underline{\alpha}}\,\frac{(R_c/a)^3}{\left\{1-(R_c/a)^3\right\}} \qquad (68)$$

a result dependent only on the magnetic Reynolds number based on the shell conductivity and the fraction of the

lunar radius occupied by core material. For frequencies sufficiently small that $k_c R_c << 1$, or for a core conductivity sufficiently small that $k_c R_c << 1$ (for $\omega = 0(10^{-5} \text{sec}^{-1})$ and $R_c = 0(10^6 \text{m})$, $\sigma_c << 10^{-1} \text{mhos/m}$), $B_1(k_c R_c) \approx 0$ and the surface magnetic field becomes

$$\frac{\underline{H}_s}{H_0}(r=a) \underset{k_c R_c \to 0}{} \underline{a}_y + (\sigma_s \mu v a) \sin\gamma \, \hat{\underline{\eta}} \frac{(\frac{1}{2} + \frac{R_c^3}{a^3})}{(1 - \frac{R_c^3}{a^3})} \qquad (69)$$

3.3 Concluding Remarks

The power spectra from lunar surface magnetometer experiments can be quantitatively evaluated using Equation (67) in conjunction with various models of the lunar conductivity. The parameters required by the theory are, in addition to knowledge of the interplanetary magnetic field and the solar wind velocity, the magnetic Reynolds number $\sigma_s \mu v a$, R_c/a and $\sigma_c \mu R_c^2$. With enough data, the possible values of these parameters should be sufficiently constrained to yield information on σ_c and consequently the temperature of the lunar interior. For the frequencies of interest and a low conductivity core $\sigma_c << 10^{-1} \text{mhos/m}$ we note that there is no indiced dipolar magnetic field (Equation (67)). The existence of a measurable induced dipolar field at the lunar surface, for the frequencies of interest, would rule out the possibility of a cold moon.

APPENDIX A

We list here the values of the coefficients

a_n^c , b_n^c , $a_n^{(1)s}$, $b_n^{(1)s}$, $a_n^{(3)s}$ and $b_n^{(3)s}$.

$$a_n^c = j_n(ka)\ \Delta_a^{-1}\ \left\{j_n(k_sR_c)q_n(k_sR_c)-h_n^{(1)}(k_sR_c)p_n(k_sR_c)\right\}$$

$$b_n^c = \frac{k_s p_n(\frac{2\pi a}{\lambda})}{k\Delta_b}\ \left\{p_n(k_sR_c)h_n^{(1)}(k_sR_c)-q_n(k_sR_c)j_n(k_sR_c)\right\}$$

$$a_n^{(1)s} = \frac{j_n(ka)}{j_n(k_sa) + R_1 h_n^{(1)}(k_sa)}$$

$$b_n^{(1)s} = \frac{k_s p_n(ka)}{k\Delta_{b'}}\ \left\{k_s^2\ h_n^{(1)}(k_sR_c)p_n(k_cR_c)-k_c^2 j_n(k_cR_c)q_n(k_sR_c)\right\}$$

$$a_n^{(3)s} = \frac{R_1\ j_n(ka)}{R_1\ h_n^{(1)}\ (k_sa) + j_n(k_sa)}$$

$$b_n^{(3)s} = \frac{k_s p_n(ka)}{k\Delta_{b'}}\ \left\{k_c^2 j_n(k_cR_c)p_n(k_sR_c)-k_s^2 j_n(k_sR_c)p_n(k_cR_c)\right\}$$

The following quantities have been used in the above formulas for the coefficients.

APPENDIX A (Con't)

$$p_n(x) = \frac{d}{dx}\left(xj_n(x)\right) \quad , \quad q_n(x) = \frac{d}{dx}\left(xh_n^{(1)}(x)\right)$$

$$\Delta_b' = k_c k_s \Delta_b = p_n(k_s a)\left\{k_s^2 h_n^{(1)}(k_s R_c) p_n(k_c R_c) - k_c^2 j_n(k_c R_c) q_n(k_s R_c)\right\}$$

$$+ q_n(k_s a)\left\{k_c^2 j_n(k_c R_c) p_n(k_s R_c) - k_s^2 j_n(k_s R_c) p_n(k_c R_c)\right\} .$$

$$R_1 = \frac{j_n(k_s R_c) p_n(k_c R_c) - j_n(k_c R_c) p_n(k_s R_c)}{j_n(k_c R_c) q_n(k_s R_c) - h_n^{(1)}(k_s R_c) p_n(k_c R_c)} .$$

$$\Delta_a = j_n(k_s a)\left\{j_n(k_c R_c) q_n(k_s R_c) - h_n^{(1)}(k_s R_c) p_n(k_c R_c)\right\}$$

$$+ h_n^{(1)}(k_s a)\left\{j_n(k_s R_c) p_n(k_c R_c) - j_n(k_c R_c) p_n(k_s R_c)\right\} .$$

APPENDIX B

The DC limit of the general solution, i.e. the limit $\omega \to 0$, is obtained by considering $k_s^2 a^2$, $k_c^2 R_c^2$ to be $0(\frac{2\pi a}{\lambda})$ as $\frac{2\pi a}{\lambda} \to 0$. The result for the magnetic field in the lunar shell is

$$\frac{\underline{H}_s}{H_0} = \underline{a}_y + \frac{(\sigma_s \mu v a)\sin\gamma \; \hat{\underline{\eta}} \left\{ \frac{r}{2R_c} \left(2 + \frac{\sigma_c}{\sigma_s}\right) - \frac{R_c^2}{r^2} \left(1 - \frac{\sigma_c}{\sigma_s}\right) \right\}}{\frac{a}{R_c} \left(2 + \frac{\sigma_c}{\sigma_s}\right) + \frac{R_c^2}{a^2} \left(1 - \frac{\sigma_c}{\sigma_s}\right)}$$

If one considers $\sigma_s/\sigma_c \ll 1$, the toroidal field is precisely the toroidal field of the time dependent interaction (aside from $e^{-i\omega t}$). The result should be compared with the toroidal term on the right hand side of Equation (66).

4.0 DC Moon-Solar Wind Interaction Using a Two Layer Moon Model

The Explorer 35 measurements (Colburn et al, 1967, and Ness et al, 1967) place an upper limit on the lunar magnetic field and the size of the lunar limb shock. The data from the magnetometer experiments indicate that at a distance of 800 km from the lunar surface, the intrinsic lunar magnetic field cannot be greater than 2 gamma (2×10^{-5} gauss). This value and the absence of a lunar bow shock can be used to set an upper limit to the unipolar interaction. In fact, it will be shown that these maximum values for the induced field are of the proper magnitude to produce an incipient shock or solar wind standoff at the lunar limb.

Following Sonett and Colburn (1967, 1968) and Hollweg (1968), we will use the concept of a unipolar generator to interpret and predict magnetic measurement effects based on the interaction between the solar wind and the moon. Following their theoretical treatment, we will use a simple two layer moon model in order to facilitate the examination of a wide range of parameters.

4.1 Interaction Model

The method generally applied is the modeling of

the moon by two spherically symmetric, homogeneous layers with an isotropic plasma for the solar wind. The driving term for the unipolar generator is the $\vec{V} \times \vec{B}_o$ electric field arising from the motion of the moon across the magnetic field lines frozen into the solar wind. The unipolar interaction is expressed in terms of solutions of the partial differential equation

$$\nabla \cdot \vec{J} = 0 \qquad (70)$$

where $\vec{J}$ is the current density vector in both the moon and the plasma. If the theoretical interaction becomes strong, an extra factor, introduced by Sonett and Colburn (1967) and called the k factor, is used to account for the deviation of the solar wind flow by the induced unipolar fields. The k factor is deduced from a magnetic field-solar wind pressure balance in which the induced field is calculated using a Biot Savart law approach. In this section the actual solution for the magnetic field at the lunar surface is obtained analytically with the assumption that the plasma conductivity

is very high so that in the plasma the only field is the incident $\vec{B}_o$ and $\bar{V} \times \bar{B}_o$ field.

Equation (70) is inadequate for a solution of the electromagnetic fields without further assumptions as to the nature of the moon, and also, proper boundary conditions at the lunar surface. In Figure 15 a two layer model for the moon is shown. With the assumption that the conductivities - σ_c , σ_s - are constants (the subscripts c and s refer to the lunar core and surface layer), it becomes a simple matter to obtain solutions for the unipolar generator in each region. With $E = -\nabla\psi$ we find that

$$\psi_c\ (r,\theta) = Ar\ \cos\theta \qquad (71)$$

$$\psi_s\ (r,\theta) = r\ \cos\theta\ (B + C/r^3) \qquad (72)$$

Associated with these solutions are the magnetic fields which in each region are given by:

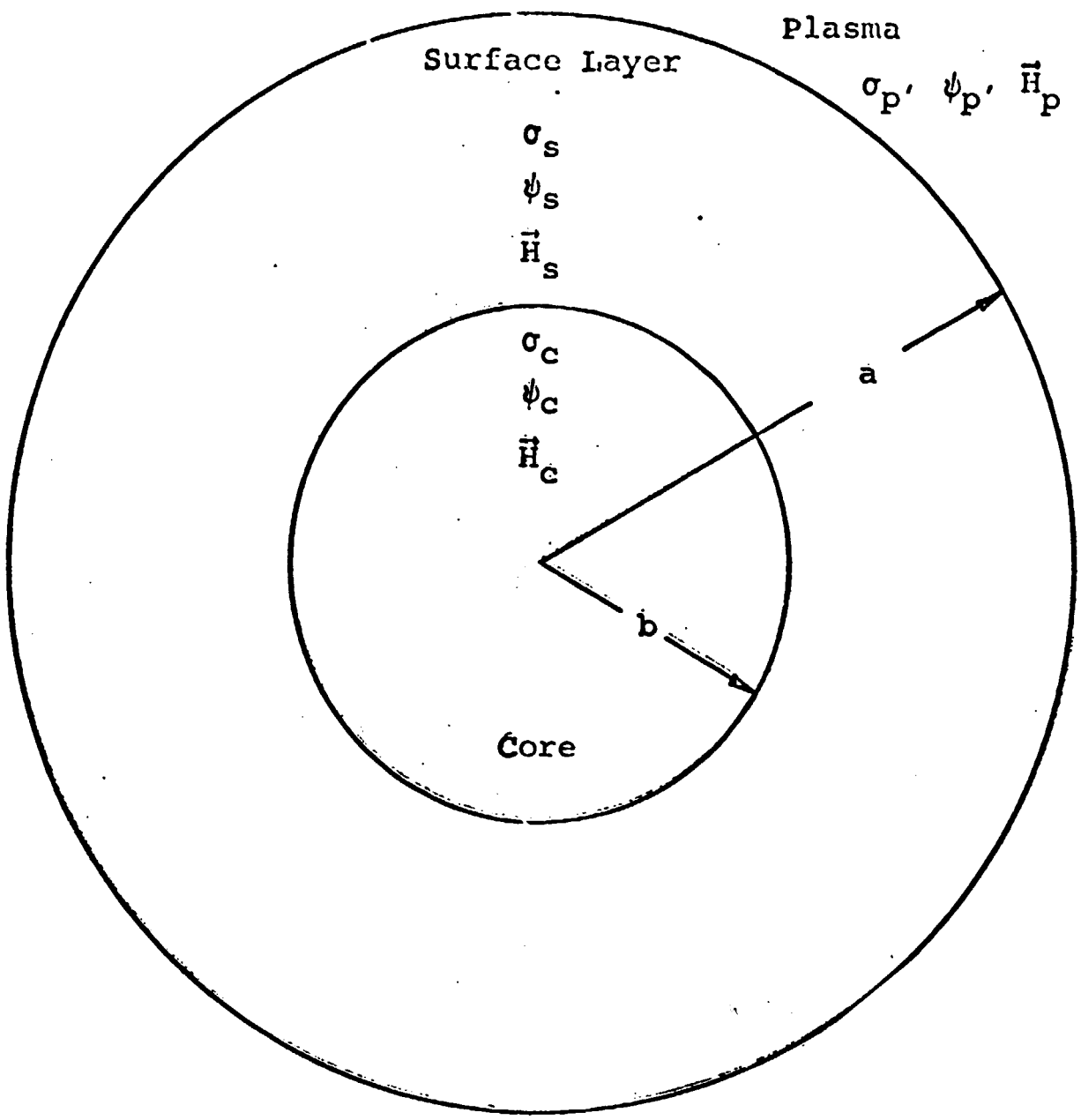

Figure 15 - Two Layer Moon Model

$$\vec{H}_c(r,\theta) = \vec{H}_o - \hat{e}_\varphi \sigma_c \, rA \sin\theta/2 \qquad (73)$$

$$\vec{H}_s(r,\theta) = \vec{H}_o - \hat{e}_\varphi \sigma_s \, r \sin\theta \, (B - 2C/r^3) \qquad (74)$$

where $\vec{H}_o = \vec{B}_o/\mu_o$ is the original magnetic field in the plasma and where $\hat{e}_\varphi$ is a unit vector in the φ-direction. The constants A, B, and C are obtained by using the continuity condition for the potentials at $r = b$ and from the condition that the normal component of the current is continuous at that boundary. This condition is simply:

$$\sigma_c \left.\frac{\partial \psi_c}{\partial r}\right|_{r=b} = \sigma_s \left.\frac{\partial \psi_s}{\partial r}\right|_{r=b} \qquad (75)$$

At $r = a$, the assumed boundary condition is:

$$\frac{1}{a} \left.\frac{\partial \psi_s}{\partial \theta}\right|_{r=a} = E_m \cos\theta \qquad (76)$$

where

$$E_m = \left| V \times B_o \right| \tag{77}$$

4.2 The Unipolar Fields

Using the continuity condition for the potential and the normal components of the current density, one can easily obtain expressions for the coefficients A, B and C:

$$A = -3\sigma_s E_m a^3/\Delta \tag{78}$$

$$B = -(2\sigma_s+\sigma_c) E_m a^3/\Delta \tag{79}$$

$$C = (\sigma_c-\sigma_s) E_m a^3 b^3/\Delta \tag{80}$$

where

$$\Delta = \sigma_c(a^3-b^3) + \sigma_s(2a^3+b^3) \qquad (81)$$

These results are identical to Hollweg's results.

4.3 The k Factor

From the experimental observation that the moon does not exhibit a magnetic bow shock, we can assert that the k factor (Sonett and Colburn, 1967 and 1968) must be much less than unity. The value of the k factor for a given solution to the unipolar problem is obtained by comparing the normal component of the solar wind pressure to the induced magnetic field back pressure. On the assumption that a fraction k of the solar wind will be turned away by the back pressure, Sonett and Colburn (1967) wrote down an expression for obtaining the k factor. This expression can be generalized to read in the coordinate frame in the moon

$$\frac{1}{2}\rho V^2 k \sin^2\theta \sin^2\varphi = (1-k)^2 B_i^2 \sin^2\theta/2\mu_o \qquad (82)$$

where

$$B_i = -\mu\sigma_s a(B-2C/a^2) \qquad (83)$$

from Equation (74). The quantities p, V and B_i are respectively the solar wind mass density, solar wind velocity, and the induced magnetic field from the unipolar generator if we did not take the solar wind deviation into account. We observe that the k factor as defined in Equation (82) is a function of the azimuth but not the colatitude. The θ dependence factors out. The k factor used by Sonett and Colburn (1967, 1968) and by Hollweg (1968) corresponds to the value $\varphi = \pi/2$. For an induced magnetic field of 4 gamma at the equator, for a solar wind density of 10 protons/cc and a proton velocity of 400 kilometers per second, we obtain a value of 2.4×10^{-3}, much less than unity.

4.4 Numerical Examples

To investigate the possibility for finding a set of parameters which could give a field of the order

of 4 gamma, the equatorial magnetic field was evaluated for a combination of values for the core and surface shell conductivities. A value of 2.82 millivolts/meter was used for the motional electric field, E_m. After the field at the surface was obtained, the k factor was calculated. In Figures 16 and 17 we have plotted $(1-k)H_i$ versus the radius of the core for two values of σ_c, 10^{-10} and 2×10^{-3} mhos per meter, and a range of values of σ_s. Additionally, we have plotted $(1-k)H_i$ as a function of k in Figure 18.

In Figure 16, the core conductivity is high, 2×10^{-3} mhos/meter, corresponding to a hot, highly conducting moon with a relatively cool insulating surface. As the surface layer thickness decreases, the equatorial magnetic field approaches a maximum value of 82 gamma. However, for all values of $\sigma_s \leq 10^{-7}$, there is a range of values of b compatible with the condition that the equatorial magnetic field be of the order of 1 gamma but no greater than, let us say, 4 gamma.

Figure 17 shows the results obtained using a cold, poorly ccnducting moon with a more conductive

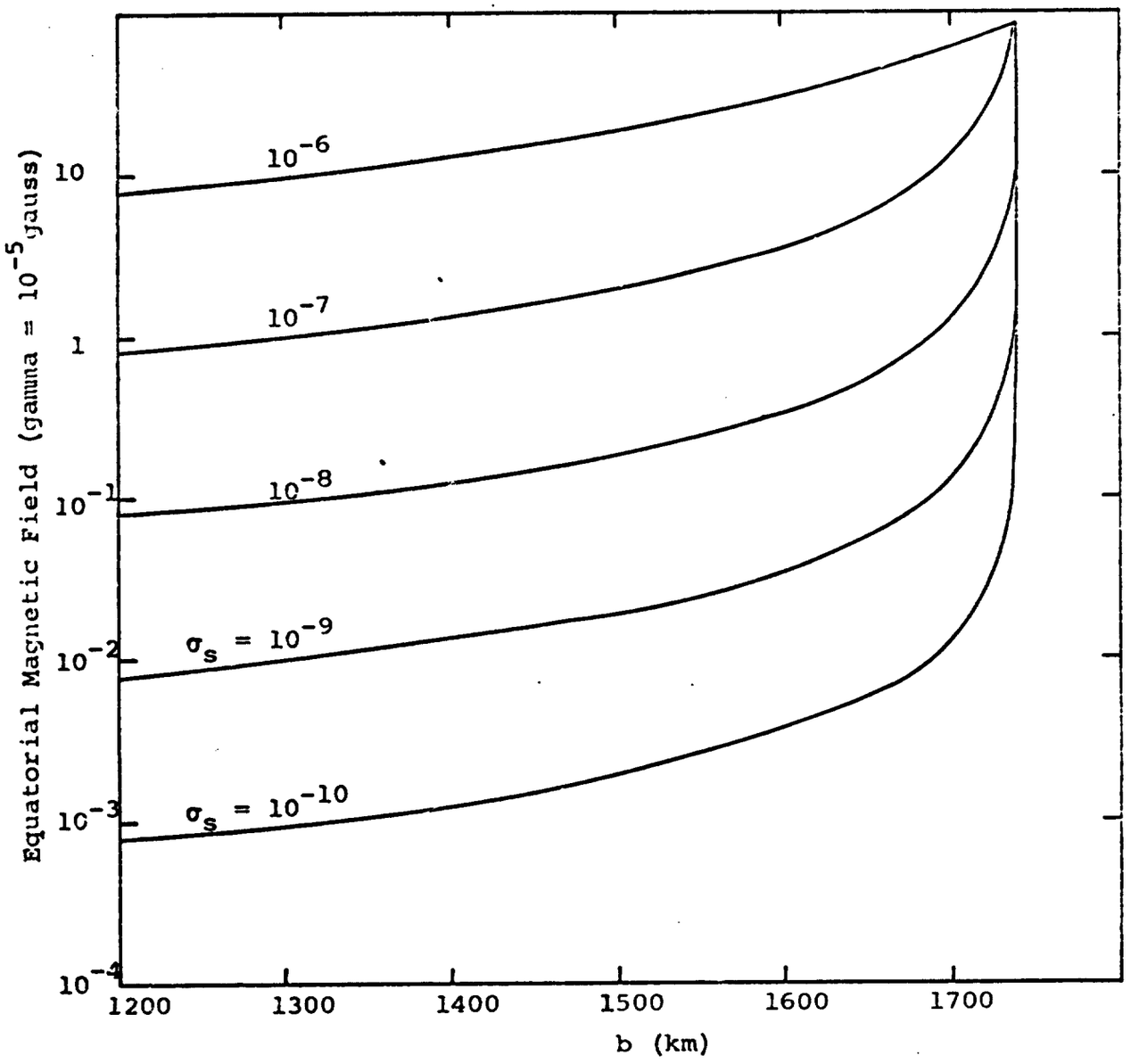

Figure 16 - Equatorial Magnetic Field vs. b
for $\sigma_c = 2 \times 10^{-3}$ mhos/meter

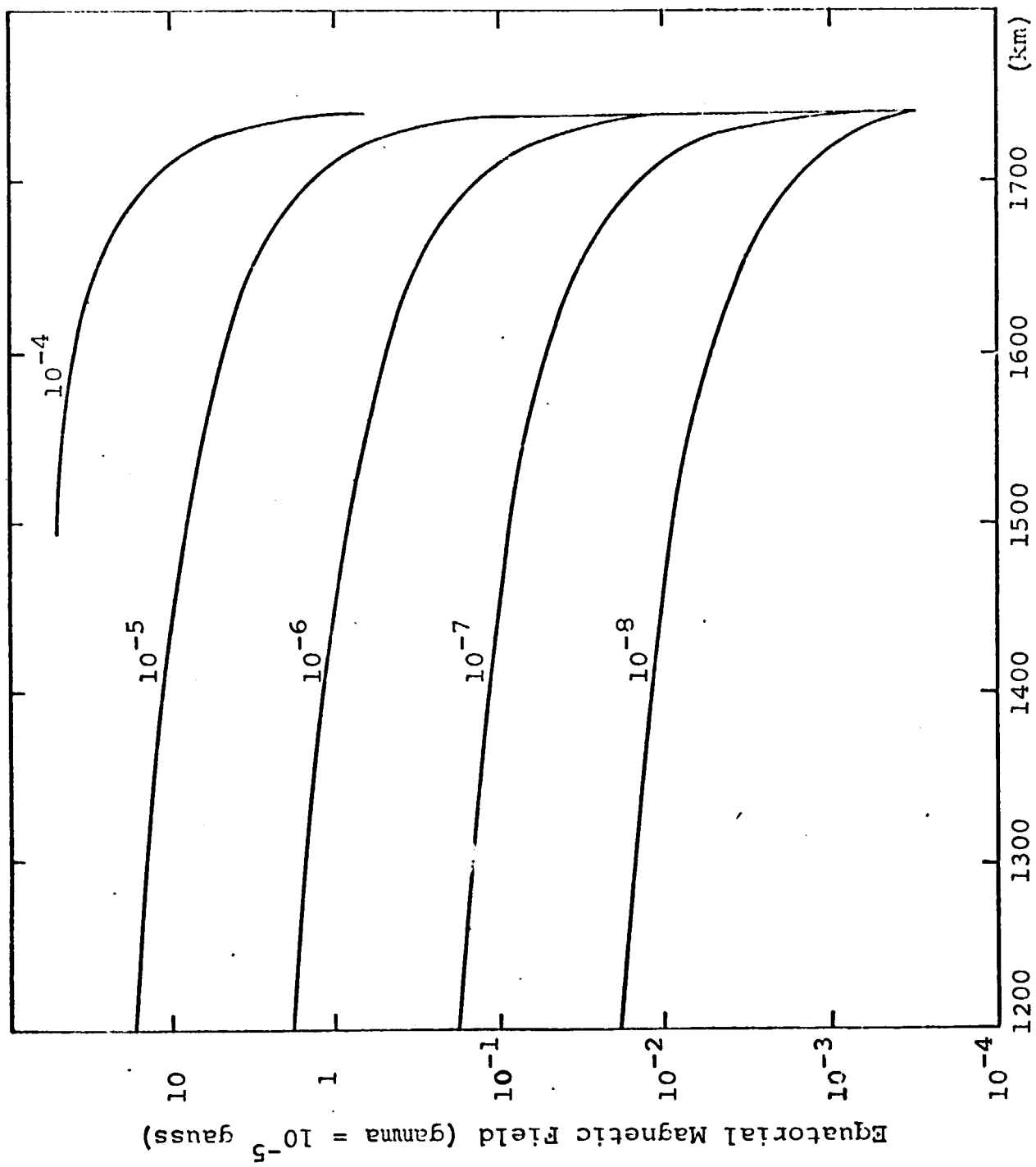

Figure 17 - Equatorial Magnetic Field vs. B

$\sigma_c = 10^{-10}$mhos/meter

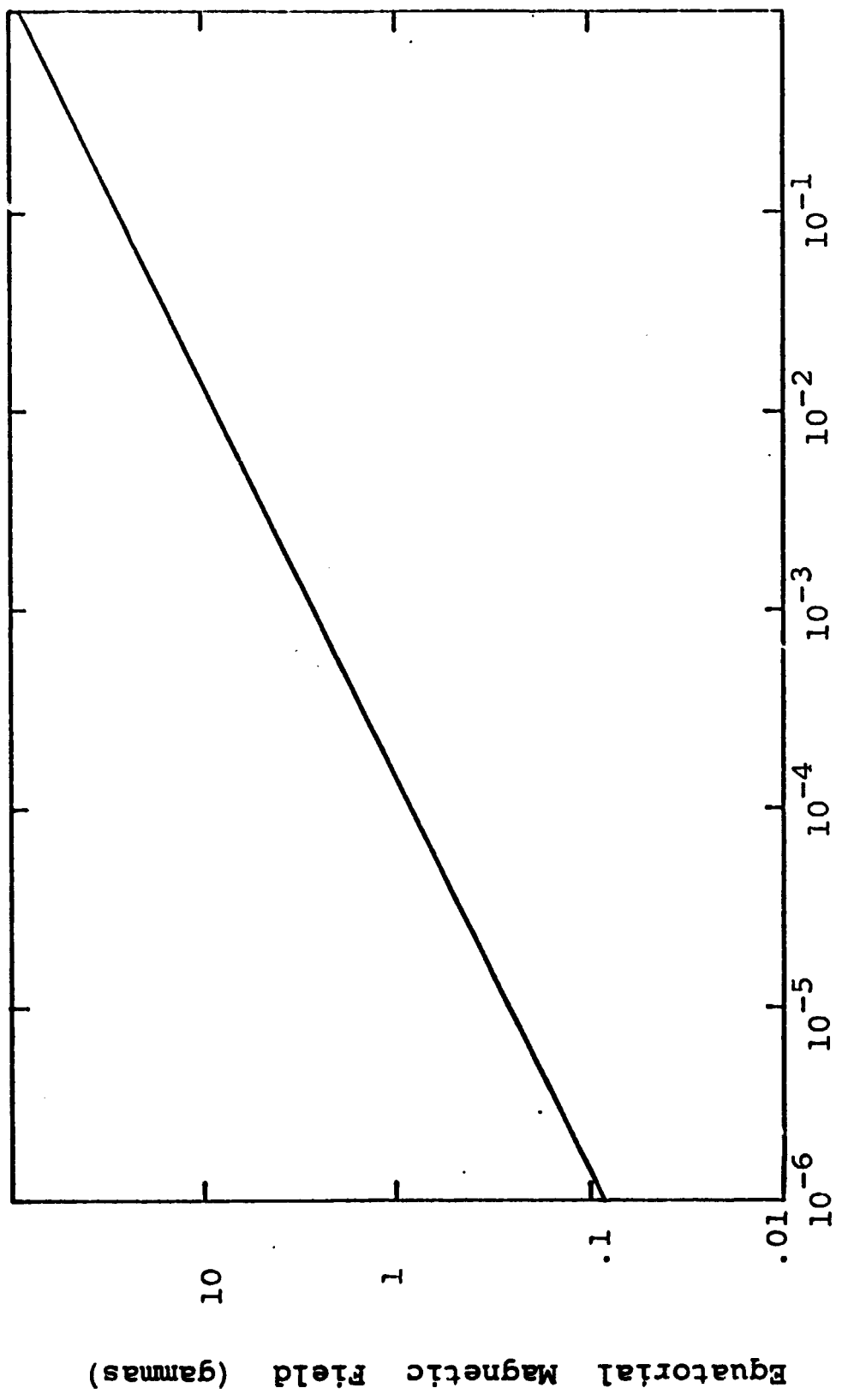

Figure 18 - k factor vs. Equatorial Magnetic Field

outer layer. For a uniform moon, $\sigma_c = \sigma_s$, a conductivity of 10^{-6} mhos/meter will produce an induced equatorial field of 3 gamma. This is in agreement with the results in Figure 16 which show that for a hot moon, the surface layer conductivity must not be greater than approximately 10^{-7} mhos/meter.

4.5 Conclusion

In the previous sections, we have indicated that an induced surface magnetic field of as much as 4 gamma is consistent with the Explorer 35 results that there is no apparent intrinsic lunar magnetic field. Further, this value is high enough to still support an incipient shock standoff near the limb of the moon. In Figures 16 and 17 we have shown calculated data for a two layer moon with a hot interior ($\sigma_c = 2 \times 10^{-3}$ mhos/meter) and a cold interior ($\sigma_c = 10^{-10}$ mhos/meter) respectively. For each case, we find that there is a range of values for the surface thickness and surface conductivity such that we can obtain the proper conditions for no observed lunar magnetic field from an orbiting magnetometer and yet also have a magnetic field large enough to produce the limb shock which has been reported

by Colburn, et al (1968) and by Siscoe, et al (1969). In addition, we may make some further speculation on the effect of a relatively high conducting layer over a two layer model with high conductivity inside and a low conductivity layer over the core. From Figure 16, we find that a hot moon with a thin surface say 20 kilometers thickness, of conductivity 10^{-9} to 10^{-10} mhos/meter will produce a negligible induced magnetic field. However, for the point of argument, let us take as a value 3.1 gamma. This is the induced field for a uniform moon with a conductivity of 10^{-6} mhos/meter. In Figure 19, we have plotted the induced magnetic field for various surface conductivities as a function of thickness for very thin layers. We note that for this case where the uniform moon already produces an induced field which is at the threshold level, a surface layer 500 meters thick with a conductivity of 10^{-3} mhos/meter barely increases the induced magnetic field. Values of 10^{-2} mhos per meter, however, will have a pronounced effect for layer thickness greater than 50 meters. It should be noted, however, that a land mass on the earth with a conductivity of 10^{-2} mhos/meter is considered to be an average value. On the moon, with constant solar baking and no atmosphere, 10^{-2} mhos/meter would appear to be a rather unlikely extreme.

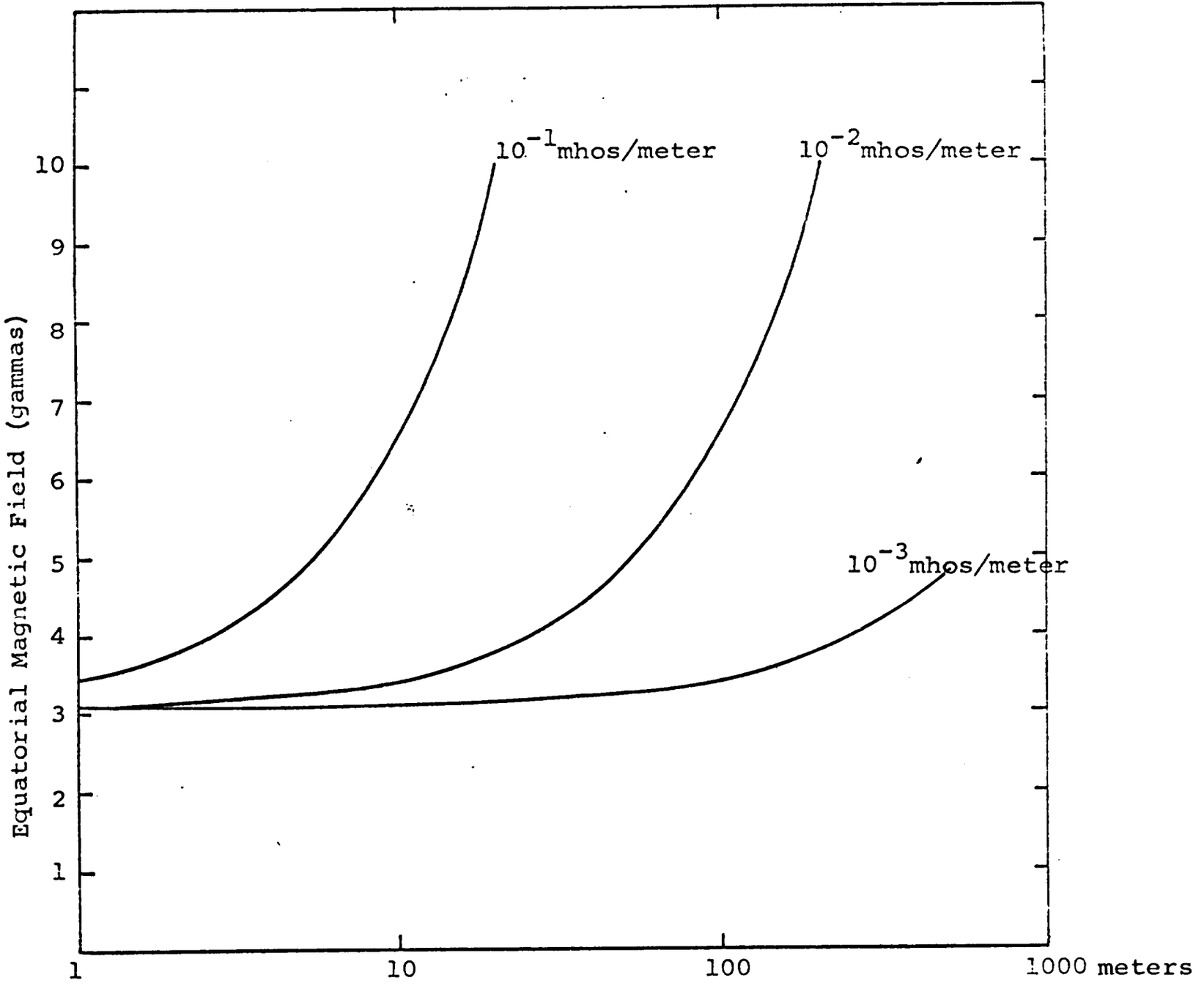

Figure 19 - Equatorial Magnetic Field vs. b (meters)
for various values of σ_s $\sigma_c = 10^{-6}$mhos/meter.

5.0 Surface Cooling for the Moon

In the computer program used to compute the thermal history of planetary bodies, MELT, a radiation-conduction balance condition, is used to determine the surface temperature:

$$-K\frac{dT}{dr} = S(T_s^4 - T_h^4) \qquad (84)$$

where K is the thermal conductivity, S is the Stefan-Boltzmann constant, T_s is the surface temperature at (r=a), and T_h is the hohlraum or space temperature. In the current version of this program and in previous versions, we have used for the hohlraum temperature the expression:

$$T_h(t) = T_o + T_{ss}\exp(-\gamma_s t) \qquad (85)$$

where T_o is normally taken as 273°K, γ_s is assumed to have

the same value as the time constant for the T Tauri number density time constant which we have been using, 1.2×10^{-6}/year, and T_{ss} is an increase over the normal space background temperature caused by the T Tauri circumstellar obscuration. In the past T_{ss} has been varied in the range

$$0 \leq T_{ss} \leq 500° \qquad (86)$$

In the program, the derivative in Eq. (84) was approximated by

$$\frac{\partial T}{\partial r} \simeq (T_s - T_n)/\Delta \qquad (87)$$

where Δ is the size of the spatial grid in the integration of the heat flow equation and T_n is the temperature at the first grid point below the surface:

$$T_n = T(a-\Delta) \qquad (88)$$

Originally this choice was independent of the time interval used in integrating the heat flow equation.

The time scale for thermalization in the heat flow equation for a distance Δ is given by

$$\tau = \rho C_p \Delta^2 / K \qquad (89)$$

For the lunar problem we used the values:

$$\rho = 3.34 \text{ grams/cc}$$
$$C_p = 1.2 \text{ joules/gram}^\circ\text{K}$$
$$K = 8 \times 10^5 \text{ joules/cm-year-}^\circ\text{K}$$
$$\Delta = 2 \times 10^5 \text{ cm}$$

With these values we find that

$$\tau = 2.0 \times 10^5 \text{ years}$$

The actual time steps used in integrating the heat flow equation during T Tauri are actually of the order of 10^3 years.

The solution for T_s for the pair of equations (84) and (87), is independent of Δt. Thus, if $\Delta t = 10^{-7}$ years or 10^5 years, we obtain the same result for T_s. In order to obtain a more accurate solution for the boundary temperature and one that will agree with theoretical predictions over some range, Δ must be sufficiently small so that the thermalization time given by Equation (89) and the computer time step are of the same order. Specifically, the distance Δ is determined by the equation:

$$\Delta = \alpha \sqrt{\frac{K\ \delta t}{\rho C_p}} \qquad (90)$$

when δt is the time step controlled by the thermal input, and where α is an as yet undetermined arbitrary constant of order unity. To fix the value of α we will compare the surface temperature which is derived from the computer program with this modification to values obtained for a suitable, soluble, theoretical model.

5.1 Theoretical Model

As a theoretical test model, we will consider the problem of a semi infinite solid, initially at a constant temperature, radiating into space. Solutions for this problem for long and short time have been obtained by Abarbanel (1960). For short times, Abarbanel gives the formula:

$$y(\tau) = 1 - 2\beta\sqrt{\frac{t}{\pi}} + 4\tau\beta^2 - 32\left(\frac{\tau}{\pi}\right)^{3/2}\beta^3 +$$

$$\frac{12}{\pi}\tau^2\beta^4 - \frac{256}{15}\beta^5\left(\frac{\tau}{\pi}\right)^{5/2} \ldots \qquad (91)$$

where $y(\tau)$ is the normalized surface temperatures at the normalized time

$$y = \frac{T}{T_o} \qquad (92)$$

$$\tau = e^2 s^2 T_o^6 \, t/K \qquad (93)$$

$$\beta = \left|1-(T_o/T_h)^4\right| \qquad (94)$$

where T_o is the initial temperature of the body, T_h is the temperature of the space into which the body is radiating and when all the other constants have already been defined. Equation (91) is exact for small τ. For large τ there is an asymtotic solution of the form

$$y(\tau) = \alpha + \frac{(1-\alpha)}{4\alpha^3} \cdot \frac{1}{\sqrt{\pi\tau}} \qquad (95)$$

where $\alpha = T_h/T_o$. From the reference paper, Eq. (95) is not a good solution until $\tau \approx 100$. For smaller values of τ, the asymtotic solution gives temperatures which are too high.

5.2 Computer Model and Results

In the introduction, it was pointed out that the spatial derivative in Equation (84) is approximated by Equation (87). In order to obtain a more reasonable approximation for short times, the spatial step in the approximation was changed from the spatial step in the heat diffusion integration to a spatial step determined from the time step used in the heat diffusion partial differential equation; e.g., Equation (90). We have set α equal to unity for all calculations. It will be seen that the results do not warrant further investigation for a better value. The results of the computer calculations are shown in Figure 20 for four different values of Δ ; 1 , 10 , 100 , 10,000 centimeters. The integration was started for each case at $t = 10^{-7}$ years with the moon at 500°C (773°K) and the space temperature, T_h , held at 0°C (273°K). The reason for four different grid sizes comes about because of computing time requirements. The maximum time step compatible with a stability criterion for the heat flow differential equation is:

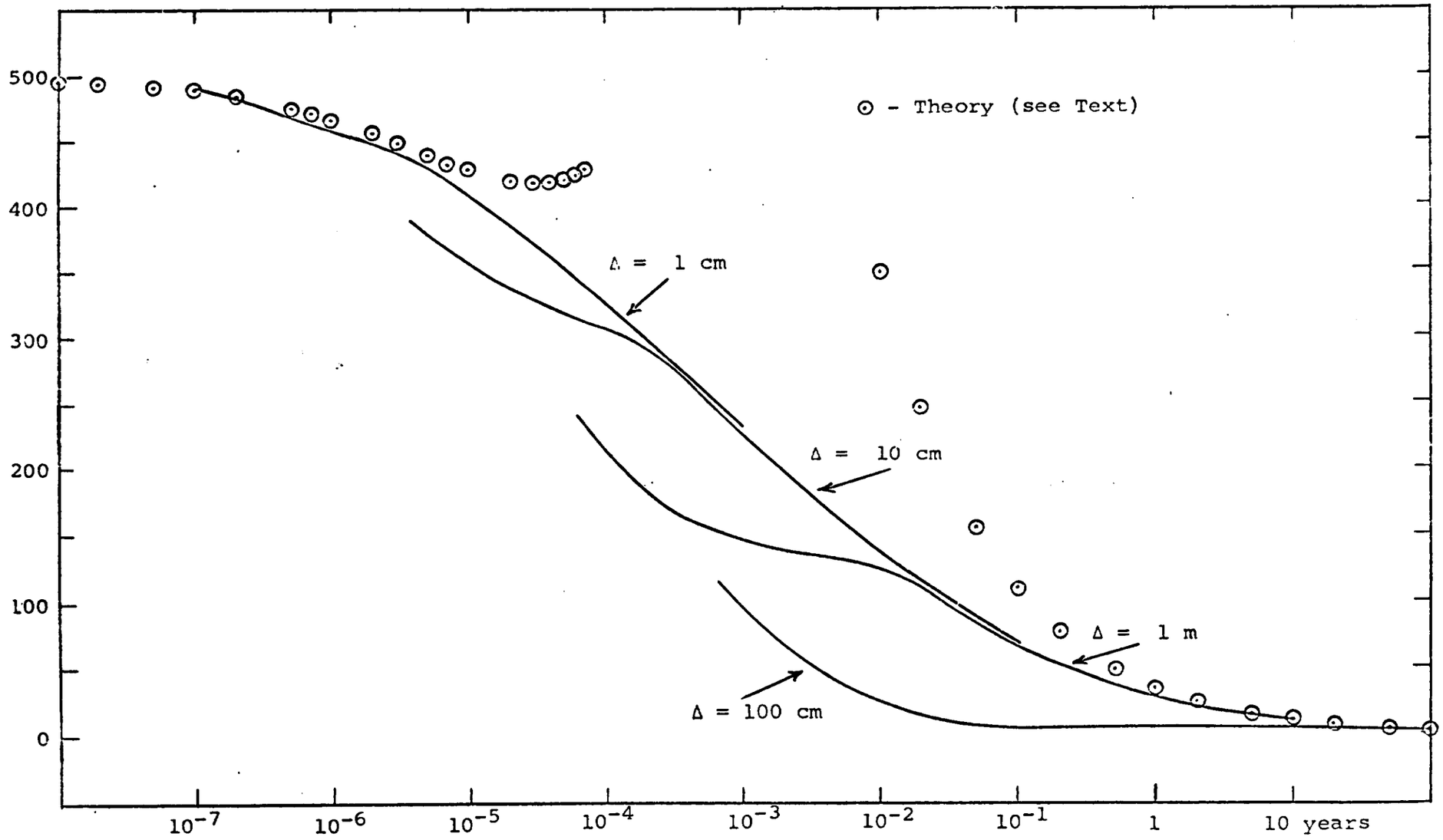

Figure 20 - Surface Temperature (°C) vs. Time (years) for the Moon - T(0) = 500°C, T_h = 0°C

$$\Delta t\Big|_{max} = \rho\, C_p\, \Delta^2/2K \qquad (96)$$

This is one-half the time step given by Eq. (89). For a spatial grid size of 1 cm, $\Delta t\Big|_{max}$ is 2.5×10^{-6} years. For very short time, up to 10^{-3} years, this small time step is not unreasonable. However, for each factor of 10 in the time for which we wish to solve the equation, we require an increase by a factor of 10 in the computer running time. Hence, we resort to larger grid sizes and consequently larger values of $\Delta t\Big|_{max}$ for cases where long time scales are important.

Now let us consider the interesting case of Figure 10. The top solid curve labeled Δ = 1 was calculated using a one centimeter space grid. The curve has a slight bow at 10^{-6} years, then follows what would appear to be a reasonable path until the computations were stopped at 10^{-3} years. The next solid curve, Δ = 10 cm, was again computed for a start time of 10^{-7} years. The calculated surface temperature is extremely inaccurate until approximately 10^{-4} years. The curves for Δ = 1 and Δ = 10 approach each other asymtotically from 3×10^{-4} to 10^{-3} years. The third curve, Δ = 100 cm, does not approach the curve Δ = 10 cm until approximately t = 10^{-2} years. Before

that, it is very much below the expected time history of the surface. Finally, the last curve, $\Delta = 10^4$ cm, approaches the $\Delta =$ 100 cm curve near the hohlraum temperature of 0°C.

There are two immediate questions which arise. First, what is the theoretically predicted surface temperature? Second, what produces the somewhat strange shape for each of the four calculated curves and why do they eventually come together when they do? The first question is easily disposed of. The theoretical results from Eqs. (92) and (95) are also shown in Figure 20. For very short time, $t < 3 \times 10^{-5}$ years, the $\Delta = 1$ cm curve closely approximates the theoretical data. The approximation for small time begins to break down for $t > 3 \times 10^{-5}$ years. At the other end of the time scale, the asymtotic formula for large time falls on the curve $\Delta = 100$ cm for $t > 5$ years. Note, that by this time, the difference between the surface temperature and the hohlraum temperature is negligible, less than 15°. For $t = 10^3$ years, the surface temperature is within 1.1° of the hohlraum temperature. From the combination of the theoretical formulas and the computer calculation, it is obvious that the approximation used in the computer program provides a more than adequate value for the surface

temperature for times greater than, let us say, 10 years.

The question of the strange shape of the curves, their inflections, still remains. A simple analysis shows that the inflections occur for times of the order of the stability time of the partial differential equation. For shorter times, the set of approximations used to obtain the derivative in the heat flow surface boundary condition of Eq. (84) is inadequate for a proper representation of the boundary condition. As the time scale reaches and then passes the maximum time step for stability, the approximate derivative given by Eq. (89) becomes a good approximation and the computer surface temperature begins to follow a proper curve.

6.0 Summary and Conclusions

6.1 The Response of the Moon to a CW Incident Electromagnetic Field

One of the major efforts during this program was the investigation and solution of the problem of the response of a two layer moon model to a CW incident electromagnetic field. This work used the combined time dependent magnetic and $V \times B$ electric fields as the source term as opposed to the earlier work of Blank and Sill (1969a). In that work only the magnetic field term was used as a driving field. The present work shows that for sufficiently low frequencies, the response to the two terms can be obtained independently. However, except for extreme conditions where the lunar surface conductivity approaches zero, both terms are necessary to provide the total solution to the response problem. Further, the accuracy of the mathematical decoupling (physically the two terms are always present) can only be determined from the broader theory presented here. Additional work still remains ahead to apply this theory to more complex lunar models using some of the mathematical techniques employed for stratified media (for an application of these techniques see Fuller and Ward, 1969).

6.2 Present Day DC Moon Solar Wind Interaction

Schwartz, Sonett and Colburn (1969) have proposed that the unipolar generator can provide a mechanism for the lunar limb shock. In Section 4.0, the two layer moon model in conjunction with the unipolar generator is used to investigate the range of values of the interior and surface electric conductivity which is compatible with the absence of a lunar bow shock. The data shows that there is a range which will produce a negligible magnetic field in terms of the magnitudes required to produce a bow shock and yet still produce high enough values at the lunar limb to slightly deflect the solar wind and, therefore, cause the observed limb shock.

6.3 T Tauri Heating Using the Unipolar Induction Generator

Early investigative efforts using the T Tauri driven unipolar generator as a fast heating source for protoplanets employed an extremely simple model for the T Tauri environment. This model environment has been contrasted in Section 2.0 with a hypothetical environment which follows more closely the observational data for T Tauri and other early type stars. In conjunction with this comparison, an effort was made to examine, at least

partially, under what conditions the high hohlraum temperature requirement might be relaxed. It was found that for the Rikitake (1966) olivine, the hohlraum temperature could be reduced to 200°C before a major decrease occurred in the fast heating stage. With an enhanced driving field, the hohlraum could be decreased still farther, below 100° C.

REFERENCES

1. Abarbanel, S. S., "Time Dependent Temperature Distribution in Radiating Solids", J. Math Phys., Vol. 39, #4, p 246 (1960).

2. Babcock, H. W. 1958, Ap. J. Suppl., 4, 141.

3. Blank, J. L and W. R. Sill, "Response of the Moon to the Time-Varying Interplanetary Magnetic Field", J. Geophys. Res., 74, 736, 1969a.

4. Blank, J. L. and W. R. Sill, J. Geophysical Research 74, #21, p 5175, 1969b.

5. Colburn, D. S., R. G. Currie, J. D. Mihalov, and C. P. Sonett, "Diamagnetic Effect of the Lunar Cavity", Science, 158, 1040, 1967.

6. Coleman, P. J., Jr., "Turbulence, Viscosity and Dissipation in the Solar Wind Plasma", Astrophys. J., 153, 371, 1968.

7. England, A. W., G. Simmons, and D. Strangway, "Electrical Conductivity of the Moon", J. Geophys. Res., 73

8. Fuller, B. D. and S. H. Ward. "Theoretical Calculation of the Electromagnetic Response of a Radially Layered Model Moon", Space Sciences Laboratory Technical Report, Series 10 Issue 24, University of California, Berkeley, 1969.

9. Hollweg, J. V., "Interaction of the Solar Wind With the Moon and Formation of a Lunar Limb Shock Wave", J. Geophys. Res., 73, 7269, 1968.

10. Iben, I. Jr. 1965, Ap J., 141, 993.

11. Johnson, F. S. and J. E. Midgley, "Notes on the Lunar Magnetosphere", J. Geophys. Res., 73, 1523, 1968.

12. Kraft, R. P. 1967, Ap. J., 150, 551.

13. Kuhi, L. V. 1964, Ap. J., 140, 1409.

14. Mestel, L. 1968, M. N., 138, 359.

15. Ness, N. F., K. W. Behannon, C. S. Scearce, and S. C. Cantarano, "Early Results From the Magnetic Field Experiment on Lunar Explorer 35", J. Geophys. Res., 72, 5769, 1967.

16. Roxburgh, I. W. 1966, Ap. J., 143, 111.

17. T. Rikitake, "Electromagnetism and the Earth's Interior" Elsevier Press (1966).

18. Schubert, G. and K. Schwartz, "A Theory for the Interpretation of Lunar Surface Magnetometer Data", to be published in "The Moon" (1969).

19. Schwartz, K., and G. Schubert, "Time Dependent Lunar Electric and Magnetic Fields Induced by a Spatially Varying Interplanetary Magnetic Field", J. Geophys. Res., 74, 4777, 1969.

20. Schwartz, K., C. P. Sonett, and D. S. Colburn, "Unipolar Induction in the Moon and a Lunar Limb Shock Mechanism", "The Moon", to be published, 1969.

21. Siscoe, G. L., E. F. Lyon, J. H. Binsack, and H. S. Bridge, "Experimental Evidence for a Detached Lunar Compression Wave", J. Geophys. Res., 74, 59, 1969.

22. Sonett, C. P. and D. S. Colburn, "Establishment of a Lunar Unipolar Generator and Associated Shock and Wake by the Solar Wind", Nature, 216, 340, 1967.

23. Sonett, C. P. and D. S. Colburn, "The Principle of Solar Wind Induced Planetary Dynamos", Phys. Earth Planet. Interiors, 1, 326, 1968.

24. C. P. Sonett, D. S. Colburn and K. Schwartz, "Electrical Heating of Meteorite Parent Bodies and Planets by Dynamo Induction from a Pre-main Sequence T Tauri Solar Wind", NATURE, Vol. 219, p. 924, August 31, 1968.

25. Sonett, C. P., D. S. Colburn, K. Schwartz and K. Keil, "The Melting of Asteroidal Parent Bodies by Unipolar Dynamo Induction from a Premordial T Tauri Sun", submitted to "Astrophysics and Space Science", Nov. 1969.

26. Stratton, J. A., Electromagnetic Theory, McGraw-Hill, New York, 1941.